Rare evidence for formation of garnet + corundum during isobaric cooling of ultra high temperature metapelites: New insights for retrograde P–T trajectory of the Highland Complex,...

Article *in* Lithos · February 2015

DOI: 10.1016/j.lithos.2015.01.015

P.L. Dharmapriya
University of Peradeniya

Sanjeewa Malaviarachchi
University of Peradeniya

Andrea Galli
ETH Zurich

Benxun Su
Chinese Academy of Sciences

Lithos 220–223 (2015) 300–317

Contents lists available at ScienceDirect

Lithos

journal homepage: www.elsevier.com/locate/lithos

Rare evidence for formation of garnet + corundum during isobaric cooling of ultrahigh temperature metapelites: New insights for retrograde *P–T* trajectory of the Highland Complex, Sri Lanka

P.L. Dharmapriya [a,b,*], Sanjeeva P.K. Malaviarachchi [a,b,*], Andrea Galli [c], Ben-Xun Su [d], N.D. Subasinghe [e], C.B. Dissanayake [e]

[a] *Post Graduate Institute of Science, University of Peradeniya, 20400, Sri Lanka*
[b] *Department of Geology, Faculty of Science, University of Peradeniya, 20400, Sri Lanka*
[c] *Department of Earth Sciences, ETH Zurich, Sonnegstrasse 5, CH-8092 Zurich, Switzerland*
[d] *Institute of Geology and Geophysics, Chinese Academy of Sciences, 100029 Beijing, China*
[e] *Institute of Fundamental Studies, Hantana Road, Kandy, Sri Lanka*

ARTICLE INFO

Article history:
Received 10 July 2014
Accepted 10 January 2015
Available online 3 February 2015

Keywords:
Garnet + corundum
UHT metamorphism
Isobaric cooling
Highland Complex
Sri Lanka

ABSTRACT

We report the occurrence of coexisting garnet + corundum in spinel- and corundum-bearing, garnet–sillimanite–biotite–graphite gneiss (pelitic granulites) from the Highland Complex (HC), Sri Lanka. In the investigated pelitic granulites, two domains such as quartz-saturated and quartz-undersaturated are distinguishable. The quartz-saturated domains consist of porphyroblastic garnet, quartz, plagioclase, alkali-feldspar and biotite flakes rimming garnet. The quartz-undersaturated domains are constituted of two generations of garnet (Grt_1 and Grt_2), sillimanite, plagioclase, alkali-feldspar, corundum, spinel and biotite. Grt_1 encloses rare Ti-rich biotite and numerous rutile needles and apatite rods. Grt_2 contains rare sillimanite and/or spinel inclusions. Corundum occurs in mutual contact with Grt_2, partially embedded at the rim or as an inclusions in Grt_2.

Thermobarometry on inclusion phases in Grt_1 indicates that during the prograde history pelitic granulites attained a *P* of 10.5–11 kbar at *T* of ~850 °C. Textural observations coupled with both pseudosections calculated in the NCKFMASHTMnO system and Ti-in-Garnet geothermobarometry suggest that peak metamorphism occurred at ultrahigh temperature (UHT) conditions of 950–975 °C and pressures of 9–9.5 kbar. Peak *T* was followed by a period of isobaric cooling that formed corundum and Grt_2 at approx. 930 °C along with exsolution of rutile needles and apatite rods in Grt_1. Thermodynamic modelling confirms that corundum appears along an isobaric cooling path at about 920–930 °C and 9–9.5 kbar. Therefore, the investigated granulites provide a rare example of post-peak crystallization of garnet + corundum along a retrograde metamorphic trajectory under UHT conditions. Thus, isobaric cooling at the base of the crust could be regarded as an alternative process to form coexisting garnet + corundum.

1. Introduction

Ultrahigh-temperature (UHT) metamorphism is characterized by extreme thermal conditions in excess of 900 °C at deep crustal levels on a regional scale. In the last decade, UHT metamorphism was recognized as one of the fundamental aspects of the Earth and became one of the most challenging tasks in metamorphic petrology (Harley, 1998). Despite being volumetrically rare in most metamorphic terrains, Mg–Al-rich metapelites are crucial for investigating UHT metamorphism as they preserve typical mineral assemblages characteristic of extreme temperature conditions namely, sapphirine + quartz (Ellis, 1980; Galli et al., 2010; Harley and Motoyoshi, 2000; Morse and Talley, 1971; Sajeev and Osanai, 2004a), orthopyroxene + sillimanite + quartz (Martignole and Martelat, 2003; Morse and Talley, 1971; Santosh et al., 2007) and osumilite (Chinner and Dixon, 1973; Ellis, 1980; Kawasaki et al., 2011; Sajeev and Osanai, 2004a). Further, many granulite terrains throughout the world have also been inferred to be UHT using other mineral assemblages such as corundum + quartz (Osanai et al., 2006; Shaw and Arima, 1996), spinel + quartz (Caporuscio and Morse, 1978; Dasgupta et al., 1995; Kawasaki et al., 2011; Sajeev and Osanai, 2004a; Santosh et al., 2006b), high-alumina orthopyroxene (Harley and Motoyoshi, 2000), orthopyroxene + corundum (Kelly and Harley, 2004; Ouzegane and Boumaza, 1996), inverted pigeonite (Sandiford and Powell, 1986; Tsunogae et al., 2002), high-fluorine

---

* Corresponding authors at: Department of Geology, Faculty of Science, University of Peradeniya, 20400, Sri Lanka. Tel.: +94 812394215, +94 783451825 (mobile).

E-mail addresses: dharmapriya1985@gmail.com (P.L. Dharmapriya), malavi@pdn.ac.lk (S.P.K. Malaviarachchi).

http://dx.doi.org/10.1016/j.lithos.2015.01.015
0024-4937/© 2015 Elsevier B.V. All rights reserved.

biotite and pargasite (Sajeev et al., 2009; Tsunogae et al., 2003) and garnet + corundum (Osanai et al., 2006; Shimpo et al., 2006).

The garnet + corundum mineral assemblage mainly occurs in pyroxene-bearing rocks (e.g., Kelsey, 2008; Kelsey et al., 2006; Kriegsman and Schumacher, 1999; Shimpo et al., 2006; Tsunogae and Santosh, 2007). This assemblage is also reported from many UHT terrains worldwide such as the Limpopo Mobile Belt in Southern-Africa (Horrocks, 1983), Higo metamorphic terrain in Japan (Osanai et al., 1998), Eastern Ghats in India (Sengupta et al., 1999), Ouzzal in Algeria (Ouzegane et al., 2003), Anapolis–Itaucu Complex in Brazil (Moraes et al., 2002) and Palghat–Cauvery Shear Zone in southern India (Shimpo et al., 2006). This assemblage has also been reported from kimberlite xenoliths (Ater et al., 1984), aluminous eclogites (Morishita et al., 2001) and Ultrahigh Pressure (UHP) rocks (Zhang et al., 2004). In pelitic granulites, the assemblage garnet + corundum is usually formed at the peak pressure during prograde heating and subsequently breaks down at decompression forming sapphirine (e.g., Baba, 2003; Kriegsman and Schumacher, 1999; Moraes et al., 2002; Ouzegane et al., 2003), cordierite–sapphirine–spinel (Ouzegane et al., 2003) or spinel–sillimanite bearing assemblages (e.g., Osanai et al., 2006; Sengupta et al., 1999), depending on the *PT*-trajectory and bulk rock composition. Therefore, coexisting garnet + corundum is rarely preserved in many pelitic rocks and its occurrence especially in pyroxene-free rocks is extremely rare in nature (e.g., Kelsey et al., 2006; Shimpo et al., 2006; Tsunogae and Santosh, 2007).

In this study, coupling textural observations with results of thermodynamic modelling of garnet–sillimanite–biotite–graphite gneisses from the central Highland Complex (HC), Sri Lanka, we report the formation of garnet + corundum during nearly isobaric cooling from UHT conditions at the retrograde path. Thus, isobaric cooling of deep crust could be regarded as alternative process to form garnet + corundum in equilibrium which remains without breaking down to retrograde minerals with uplift.

2. Geology of Sri Lanka

Based on Nd-model ages (Milisenda et al., 1988, 1994) the Proterozoic basement of Sri Lanka has been subdivided into four lithotectonic units (Cooray, 1994; Kröner et al., 1991): the Highland Complex (HC), the Wanni Complex (WC), the Vijayan Complex (VC) and the Kadugannawa Complex (KC) (Fig. 1a).

The HC basement yields U–Pb zircon and Nd-model ages of 2000–3400 Ma and a metamorphic age of ~550 Ma (Malaviarachchi and Takasu, 2011a; Milisenda et al., 1988, 1994; Santosh et al., 2014) and is composed of granulitic meta-quartzites, marbles, calcsilicates and metapelitic gneisses, intimately associated with charnockites (e.g., Cooray, 1994; Mathavan and Fernando, 2001; Perera, 1984). According to geochronological reviews in Hö1zl et al. (1994) and Kröner et al. (1994), deposition of sediments of the HC took place from 3200 Ma to 1900–2000 Ma. Most of the granitoid plutons, presently exposed as orthogneisses, intruded at 1800–1900 Ma and 670 Ma. Hence, the HC represents a 2000–3000 Ma old crust. The HC was metamorphosed under regional granulite facies conditions between 610 and 550 Ma during assembly of the Gondwana Super Continent (Hö1zl et al., 1991, 1994; Kröner et al., 1994). In the HC, metamorphic pressures and temperatures decrease from 8–9 kbar and 800–900 °C in the east and southeast to 4.5–6 kbar and 600–700 °C in the southwest (Dharmapriya et al., 2014; Prame, 1991; Faulhaber and Raith, 1991; Kriegsman and Schumacher, 1999; Malaviarachchi and Takasu, 2011b; Raase and Schenk, 1994; Schumacher and Faulhaber, 1994). Evidences of UHT metamorphism have been reported only from few localities in the central Highland Complex (Kriegsman and Schumacher, 1999; Osanai, 1989; Osanai et al., 2000, 2006; Sajeev and Osanai, 2004a; Sajeev et al., 2007, 2010) and rarely in the southwestern part (Sajeev and Osanai, 2004b) from pelitic, mafic and quartzo-feldspathic granulites. Estimated UHT conditions range between 925 and

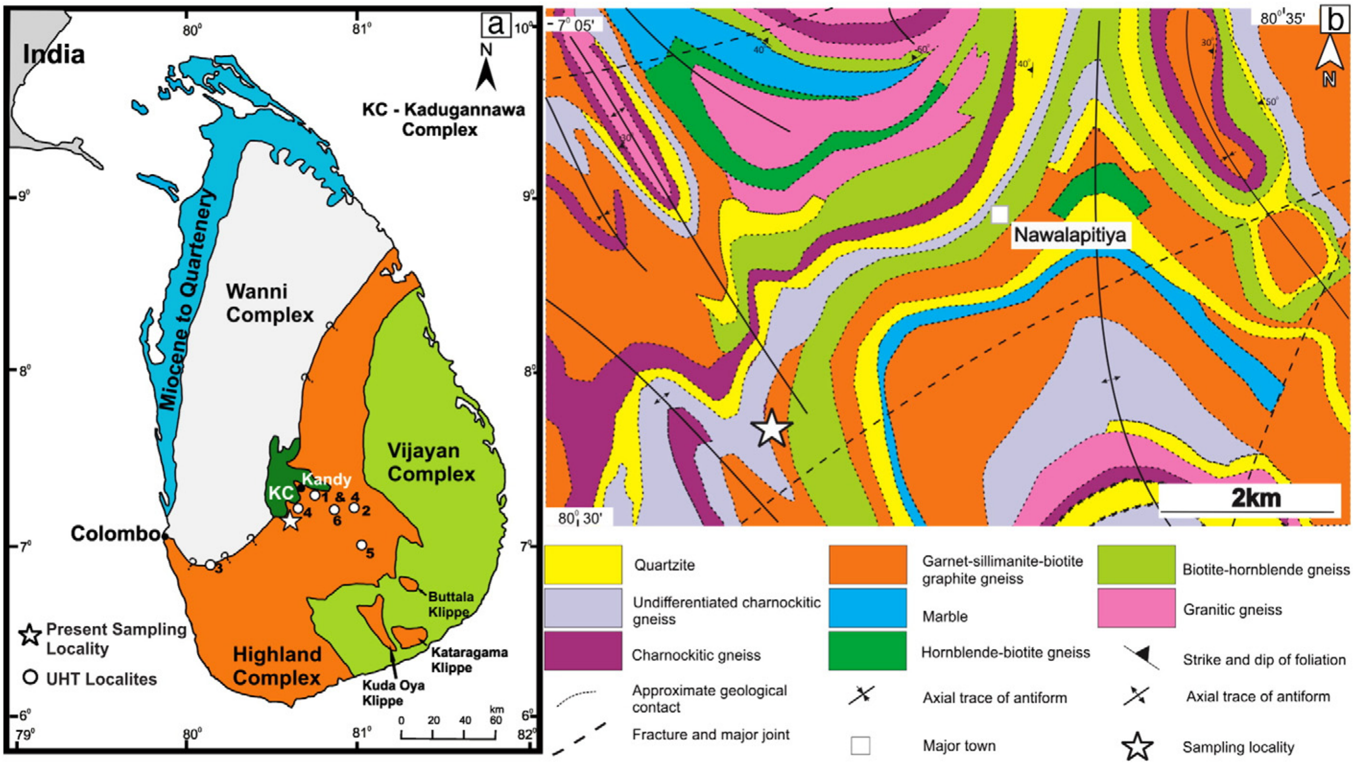

Fig. 1. (a) Geological map of Sri Lanka with litho tectonic subdivision (after Cooray, 1994). Sampling locality is shown by a star. Reported UHT localities are shown by circles: 1. Osanai (1989): $T > 900$ °C; 2. Kriegsman and Schumacher (1999): $T = 830$ °C; 3. Sajeev and Osanai (2004a): $T = 950$ °C: 4. Sajeev and Osanai (2004b): $T = 1150$ °C; 5. Osanai et al. (2006): $T > 1000$ °C and 6. Sajeev et al. (2007): $T = 925$ °C. (b) Detailed geological map of the sampling area around Nawalapitiya (central part of the Highland Complex), modified after the published map of the Geological Survey Department of Sri Lanka (1996).

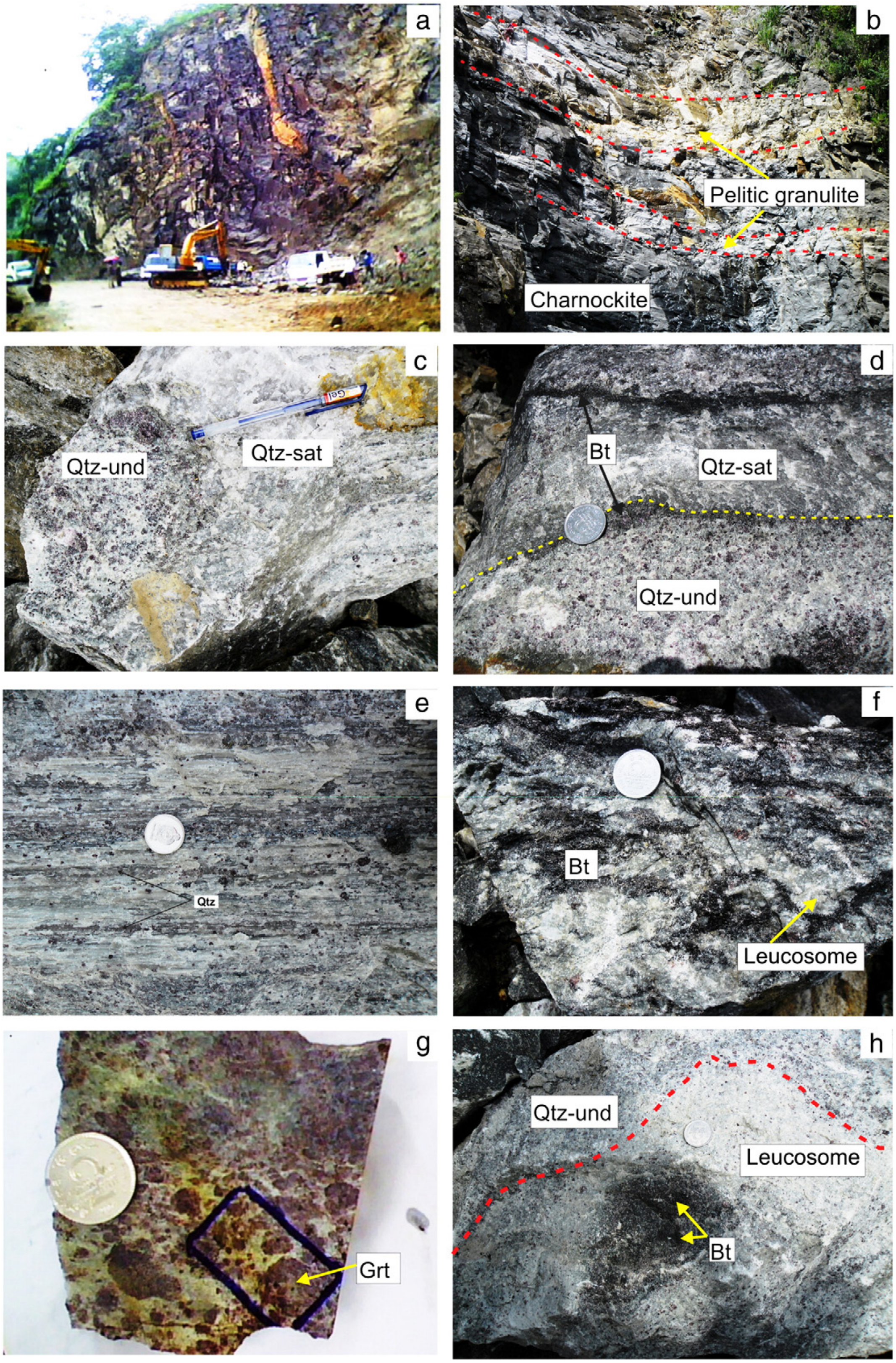

Fig. 2. (a) Exposure of investigated pelitic granulites at the quarry site; (b) intercalation of pelitic granulite bands and charnockites; (c) block showing the field relation between the quartz-undersaturated domains (Qtz-und) and the quartz-saturated domains (Qtz-sat); (d) block of quartz-undersaturated domain (Qtz-und) and quartz-saturated domain (Qtz-sat) with formation of retrograde biotite nabs parallel to major foliation at the boundary between two domains; (e) a rock slab of strongly sheared quartz-saturated domain of pelitic granulite; (f) quartz-saturated domains in pelitic granulites showing evidence for melt-leucosomes; (g) rock slab of quartz-undersaturated domain and (h) rock fragment of quartz-undersaturated domain containing clusters of retrograde biotite and feldspar bearing leucosomes.

1150 °C at a P of 9 and 12.5 kbar (Kriegsman and Schumacher, 1999; Osanai et al., 2006; Sajeev and Osanai, 2004a, b; Sajeev et al., 2007, 2010).

The WC yields U–Pb zircon and Nd model ages of 1000–2000 Ma (Milisenda et al., 1988, 1994; Santosh et al., 2014) and is constituted of orthogneisses and migmatitic ortho and paragneisses, which have been metamorphosed under granulite to amphibolite facies conditions (Kröner et al., 1991) together with some post-tectonic granites (e.g., Fernando and Iizumi, 2001). Estimated P–T conditions are $P = 3.5$–7.5 kbar and $T = 600$–900 °C (Faulhaber and Raith, 1991; Schenk et al., 1991).

The VC rocks have U–Pb zircon and Nd-model ages of 1100–1800 Ma (Kröner et al. 2013; Milisenda et al., 1988, 1994). It mainly comprises 1000–1100 Ma old calc-alkaline granitoid gneisses, migmatitic orthogneisses and minor metasedimentary enclaves, such as meta-quartzite and calcsilicates (Kehelpannala, 1997; Kröner et al., 2012) predominantly metamorphosed under upper amphibolite-facies conditions.

Rocks of the KC display U–Pb zircon ages of ~900 Ma and is composed of hornblende- and biotite-bearing orthogneisses, gabbros, diorites, granodioritic to granitic gneisses, charnockites, enderbites and minor metasediments (Kröner et al., 2003; Malaviarachchi and Takasu, 2011b; Santosh et al., 2014; Willbold et al., 2004). The KC has been separated from the other units (Cooray, 1994; Kröner et al., 1991). However, due to many similarities in lithology, structures and geochronology, some authors consider the KC as a part of the WC (e.g., Kehelpannala, 1997; Kröner et al., 2012). Recently, Santosh et al. (2014) argued that the KC is part of a disrupted huge arc magma chamber that was exhumed and transposed along the margin of the WC.

3. Field relations and sample description

Corundum- and spinel-bearing garnet–sillimanite–biotite–graphite gneisses (hereafter referred to as pelitic granulites) were collected from a quarry close to the city of Nawalapitiya, in the proximity of the contact between the HC and KC (Fig. 1a and b). This area mainly consists of strongly deformed pelitic gneisses, charnockitic gneisses, quartzites, hornblende–biotite gneisses, biotite–hornblende gneisses, marbles and orthogneisses (Fig. 1b).

The studied pelitic granulite occur as fresh, light coloured bands (about 2 –> 4m thickness, Fig. 2a and b) intercalated with charnockitic gneisses composed of garnet, orthopyroxene, hornblende, biotite, plagioclase, alkali-feldspar and quartz. In the pelitic granulites, two compositional domains are macroscopically distinguishable: quartz-saturated domains, which define the major foliation of the rock, and quartz-undersaturated domains, which occur as patches (15 cm–>1 m in diameter) within the quartz-saturated domains (Fig. 2c and d).

Quartz-saturated domains consist of stretched quartz (up to 5 cm in length, Fig. 2e), re-crystallized plagioclase and alkali-feldspar, hypidiomorphic to xenomorphic garnet-porphyroblasts (0.25–4 cm in diameter) and tiny, acicular biotite flakes occurring as thin nabs parallel to the main foliation (Fig. 2d), up to 5 cm thick patches (Fig. 2f) around porphyroblastic garnet. Thin nabs and irregular patches of biotite are associated with feldspar- and quartz-rich leucosomes (Fig. 2f) and may have grown through back-reactions with melt during retrogression.

Quartz-undersaturated domains (Fig. 2c, d, g and h) consist of numerous, up to 4 cm big, hypidiomorphic to xenomorphic garnet-porphyroblasts, sillimanite, plagioclase, corundum, alkali-feldspar, and minor biotite around garnet-porphyroblasts (Fig. 2g) or occasionally as clusters (up to 6 cm wide, Fig. 2h). Similar to quartz-saturated domains, tiny biotite clusters associated with feldspar-rich leucosomes (Fig. 2h) could probably have formed from the rock interaction with melt during retrogression.

Both domains contain minor amounts of medium-grained graphite flakes (0.2–0.7 cm) and anhedral, coarse-grained (up to 0.5–1.5 cm)

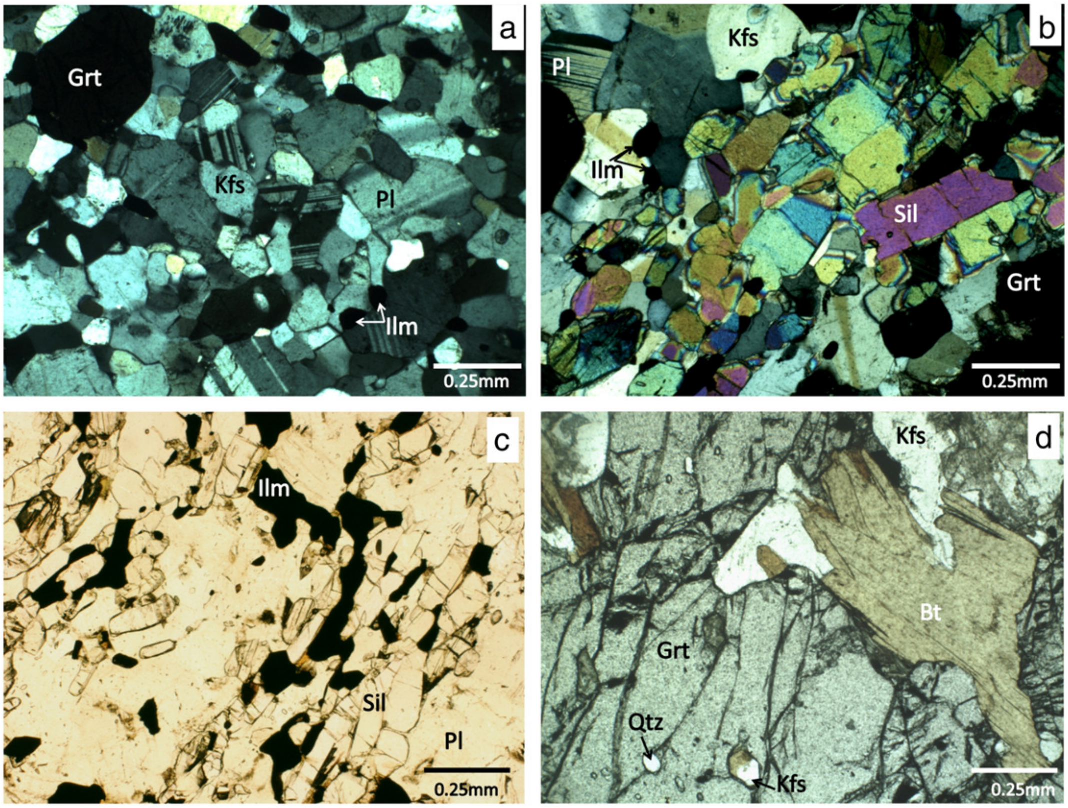

Fig. 3. Photomicrographs showing the textural features present in the matrix of the quartz-undersaturated domain: (a) recrystallized feldspars (CPL); (b) preferred orientation of acicular sillimanite needles (CPL); (c) coexistence of ilmenite with sillimanite (PPL) and (d) biotite rim around garnet (Grt_1).

pyrite crystals. Late, thin quartz veins and pegmatite dykes (<5 cm thick) crosscut the main foliation. A general strike/dip of the rock foliation is N24°W/11°NE.

4. Petrography

4.1. Quartz-undersaturated domains

The matrix of the quartz-undersaturated domains comprises garnet, plagioclase, perthitic alkali-feldspars and sillimanite as the major minerals, corundum, spinel, biotite, ilmenite, pyrite and graphite as the minor mineral phases and zircon as an accessory mineral.

Garnet occurs in two textural settings: i) coarse- to medium-grained Grt_1 (0.5–3 cm in diameter) which encloses numerous rutile needles and apatite rods, and ii) medium- to fine-grained Grt_2 (0.25–1 cm in diameter) which always occurs associated with corundum and contains sillimanite and/or spinel inclusions. Plagioclase and alkali-feldspar frequently occur as re-crystallized clusters (Fig. 3a). Sillimanite shows a preferred orientation representing the major mineral lineation on the foliation plane (Fig. 3b and c). Locally, plenty of ilmenite grains are in coexistence with sillimanite (Fig. 3c). Biotite occurs as inclusion in Grt_1 (Bt_1) or elongated, up to ~0.5 mm flakes (Bt_2) rimming garnet (Fig. 3d).

4.1.1. Textures associated with Grt_1

Bt_1 inclusions are encountered from the core to the mantle area (Fig. 4a–f). Rarely, relatively coarse-grained skeletal biotite grains (up to 0.6 cm) are present in the core area of porphyroblastic garnet (Fig. 4g). Only a few quartz inclusions occur exclusively within the mantle area (Fig. 4c, d, e and f) and may contain tiny rutile or plagioclase + alkali-feldspar inclusions (Fig. 4f). Clusters and oriented needles and rods of rutile (Fig. 4a, b, c, d, e, f, and h) and apatite (Fig. 4 a, b, c, d, e and f) occurring from the core to the rim area are

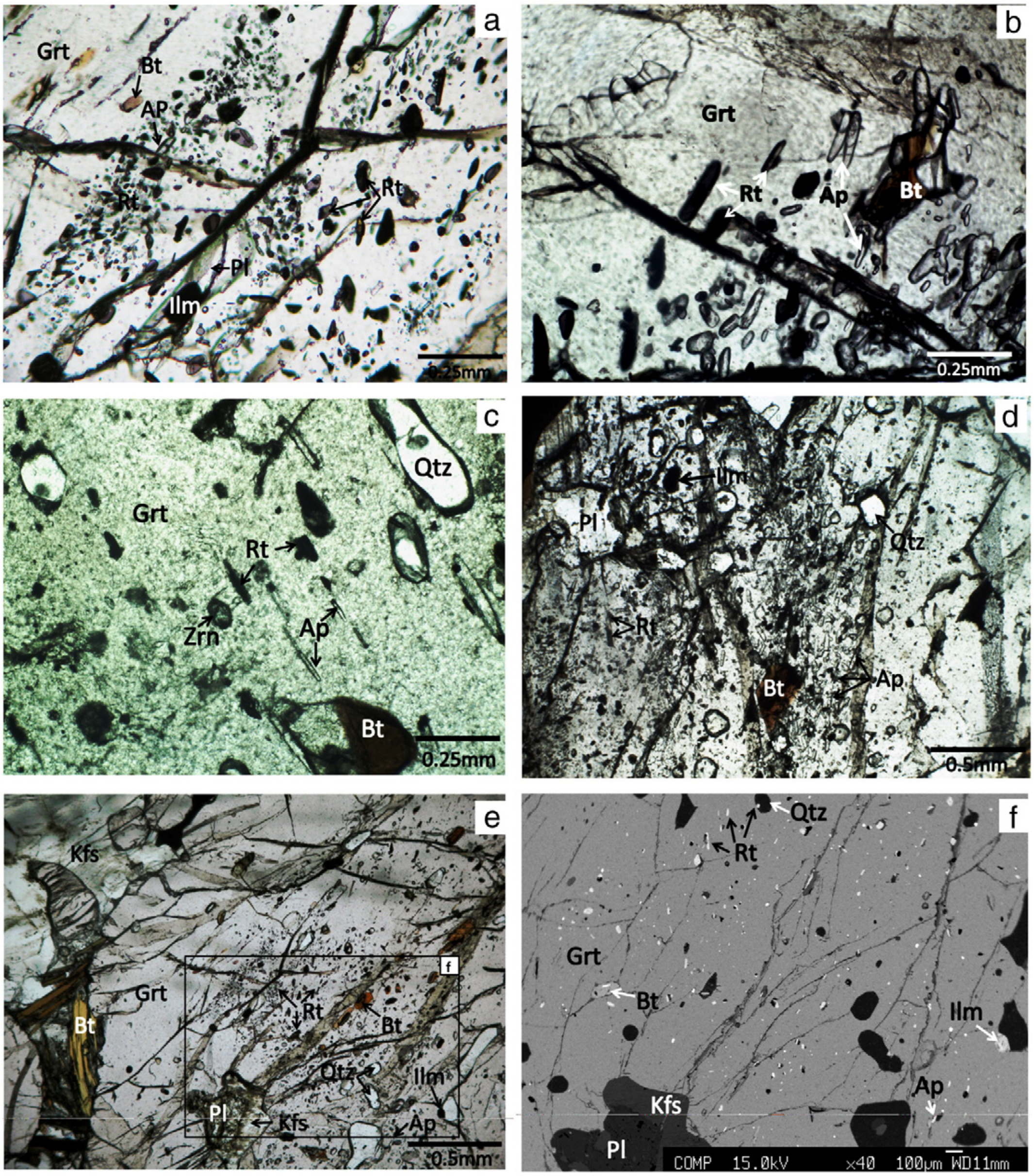

Fig. 4. Photomicrograph showing the textural features of Grt_1: (a) PPL view of tiny clusters of rutile needles, apatite rods and ilmenite inclusions in garnet; (b) medium-size rutile needles and apatite rods in mantle area of garnet; (c) oriented rutile needles and apatite rods in mantle area of garnet; (d) oriented apatite rods with minor rutile from core to rim in garnet; (e) distribution of rutile clusters from core to lower mantle of garnet; (f) backscattered image of the bottom right hand part of the garnet shown in (e); (g) inclusion of skeletal biotite within the core area; (h) oriented rutile needles in two well defined directions (dashed arrows indicate the directions of rutile needles); (i) tiny sillimanite needles in the mantle area under the gypsum plate; (j) fine-grained spinel inclusions in the rim area.

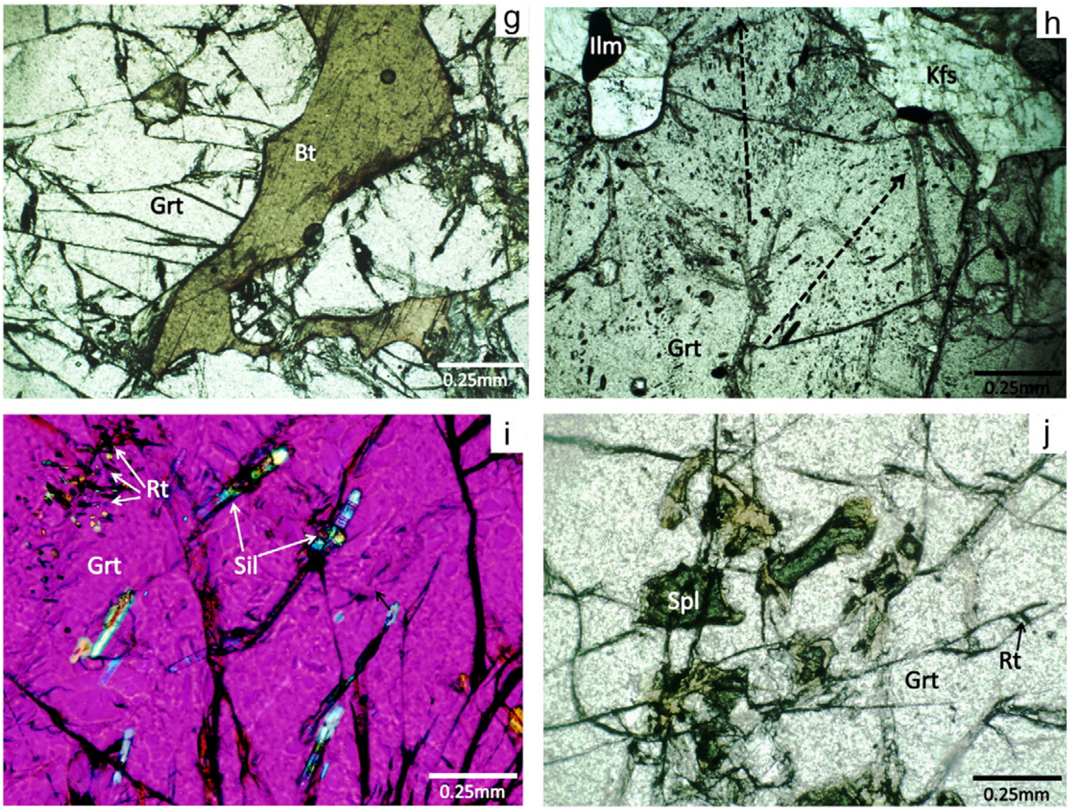

Fig. 4 (*continued*).

characteristic of Grt_1. The size of rutile needles varies from <50 μm to about 200 μm, while apatite rods are relatively larger (100 μm–350 μm). Often, ilmenite inclusions of variable sizes (<100 μm–500 μm) are associated with rutile needles (Fig. 4a, d, e and f). Locally, tiny rutile needles are oriented in two preferred directions with an angle of about 45° (Fig. 4h) suggesting that rutile is directly exsolved from Grt_1 and is not trapped-inclusions. Less commonly, tiny sillimanite needles present in the mantle to the rim of Grt_1 are oriented oblique to sillimanite in the matrix (Fig. 4i). Rarely, spinel inclusions are present in the mantle and rim area of Grt_1 (Fig. 4j).

4.1.2. Textures associated with Grt_2

Commonly, Grt_2 is in contact with corundum in the rock matrix or displays corundum inclusions (Fig. 5a to g). Corundum is also found as partially embedded grains in the rim area (Fig. 5a, b and c). In the sillimanite-absent parts of the rock matrix, subhedral and anhedral, 0.5–1.25 cm medium to coarse-grained corundum occur associated with Grt_2, two feldspars ± spinel ± ilmenite (Fig. 5a, b, and h). In the sillimanite-present/spinel-absent parts, corundum coexists with Grt_2, two feldspars ± sillimanite ± ilmenite (Fig. 5d, e and f). Rarely, needle-shaped corundum grains are observed adjacent to sillimanite (Fig. 5f), while rare coarse-grained, up to 3.5 cm large, subhedral corundum grains coexist with Grt_2 (Fig. 5g). Usually, corundum contains ilmenite (Fig. 5g) and rarely tiny spinel inclusions (Fig. 5h). Compared to Grt_1, Grt_2 contains little inclusions of rare corundum, sillimanite and spinel ± plagioclase (Fig. 5a, b, d e and g) and lacks biotite, rutile and apatite.

4.2. Quartz-saturated domains

The rock matrix of the quartz-saturated domains is composed of numerous, fine- to coarse-grained (0.25 mm–3 cm in diameter), hypidiomorphic to xenomorphic garnet porphyroblasts, stretched quartz (up to 5 cm in length, Fig. 6a), strongly re-crystallized plagioclase and alkali-feldspars (Fig. 6b) as the major constituents, pyrite, ilmenite and graphite as the minor phases and zircon and apatite as accessories. Garnet-porphyroblasts contain quartz, plagioclase and alkali-feldspar inclusions and, in minor amounts, biotite (Bt_1) and ilmenite (Fig. 6c). Occasionally, tiny (up to 3 mm in size), late biotite grains (Bt_2) are observed, probably formed as retrograde products since they are associated with leucosomes (Fig. 2f). Rarely, biotite at the rim of garnet can also be identified indicating hydration of garnet during retrogression (Fig. 6d).

5. Mineral chemistry and whole rock chemistry

5.1. Mineral chemistry

Mineral compositions were analyzed using a JEOL JXA8100 electron probe microanalyzer (EPMA) at the Institute of Geology and Geophysics, Chinese Academy of Sciences, Beijing, China. All analyses were carried out using an accelerating voltage of 15 kV and 10 nA beam current, 3 μm beam spot and 10–30 s counting time on peak. Natural jadeite [$NaAlSiO_6$] for Na, Al and Si, rhodonite [$MnSiO_3$] for Mn, sanidine [$KAlSi_3O_8$] for K, garnet [$Fe_3Al_2Si_3O_{12}$] for Fe, Cr-diopside [$(Mg, Cr)CaSi_2O_6$] for Ca, olivine [$(Mg, Fe)_2SiO_4$] for Mg and synthetic (rutile for Ti, 99.7% Cr_2O_3 for Cr, Ni_2Si for Ni) minerals were used for standard calibrations (Su et al., 2012). Matrix corrections were based on the ZAF procedure. The precisions of all analyzed elements are better than 98.5%. Mineral abbreviations are after Kretz (1983).

5.1.1. Garnet

Both Grt_1 and Grt_2 in quartz-undersaturated domains are mainly almandine–pyrope solid solutions, with only small amounts of grossular, spessartine and andradite components (Table 1). Grt_1 shows slight compositional zoning of Fe, Mg and Ca. Grt_1 cores are slightly depleted in the almandine component, while pyrope content shows behavior opposite to almandine (Table 1). The X_{Grs} is ~0.05 within garnet cores and

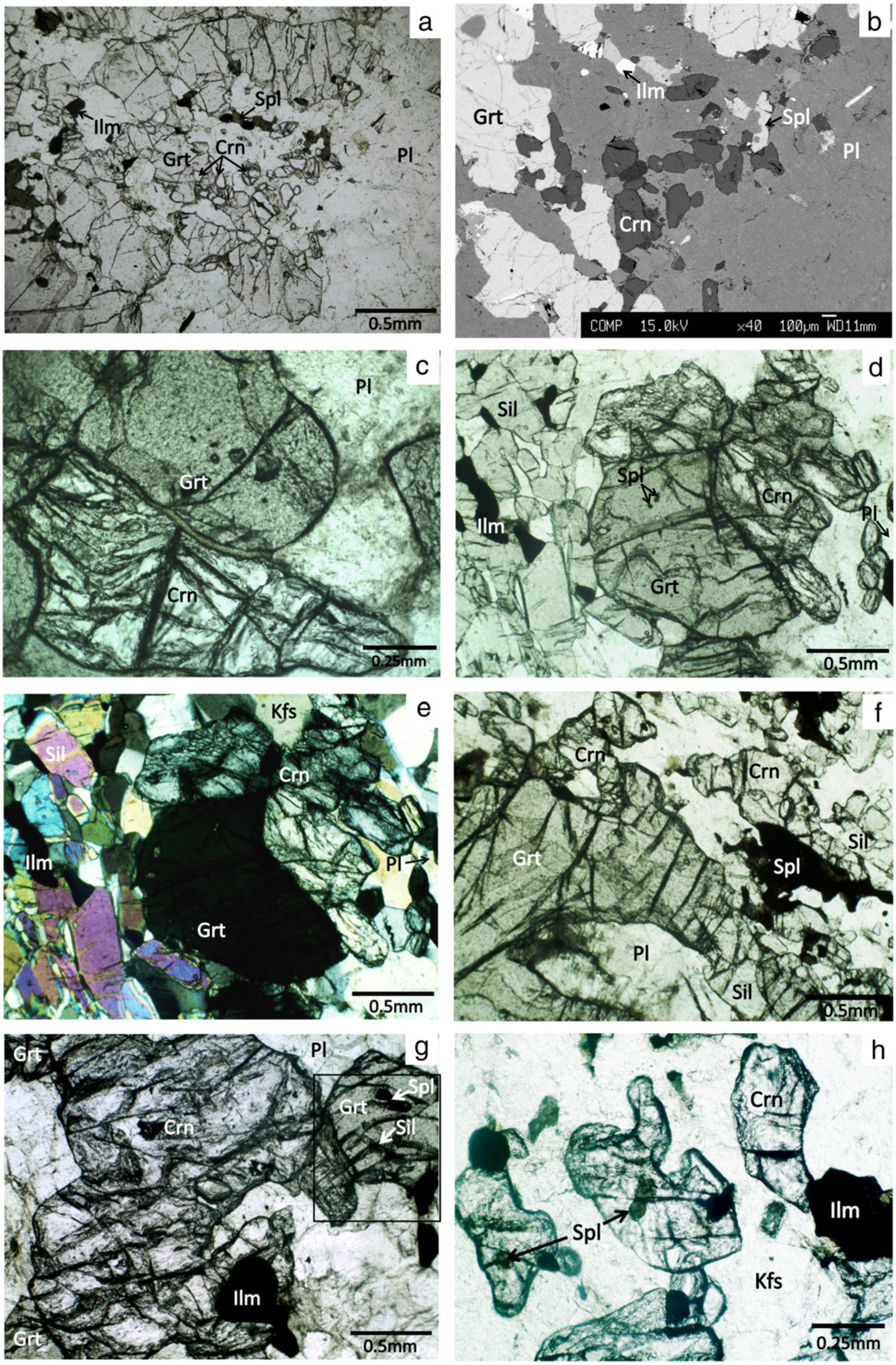

Fig. 5. Photomicrograph showing the main textural features associated with Grt$_2$: (a) anhedral fine- to medium-grained corundum coexisting with Grt$_2$ and Spl and corundum inclusions in garnet; (b) backscattered image of the image (a); (c) and (d) direct coexistence of garnet + corundum. Occurrence of sillimanite in the matrix and spinel as inclusion in garnet are also shown; (e) CPL view of the image (d); (f) matrix showing garnet + corundum associations with spinel and sillimanite; (g) coexistence of coarse-grained corundum with medium-size garnet and (h) tiny spinel inclusions within corundum.

it slightly increases towards the rim up to X_{Grs} ~ 0.07. Grt$_1$ displays relatively high Ti content ($TiO_2 = 0.052–0.100$ wt.%, Table 1). The average composition of Grt$_1$ ranges from $Alm_{57.7}Prp_{34}Grs_{4.6}5Sps_{0.7}Adr_3$ within the core to $Alm_{60.1}Prp_{33}Grs_{7.2}Sps_{0.7}Adr_0$ at the rim (Table 1). In contrast, Grt$_2$ cores are slightly enriched in almandine component and depleted towards the rim (Table 1). The pyrope content shows behavior

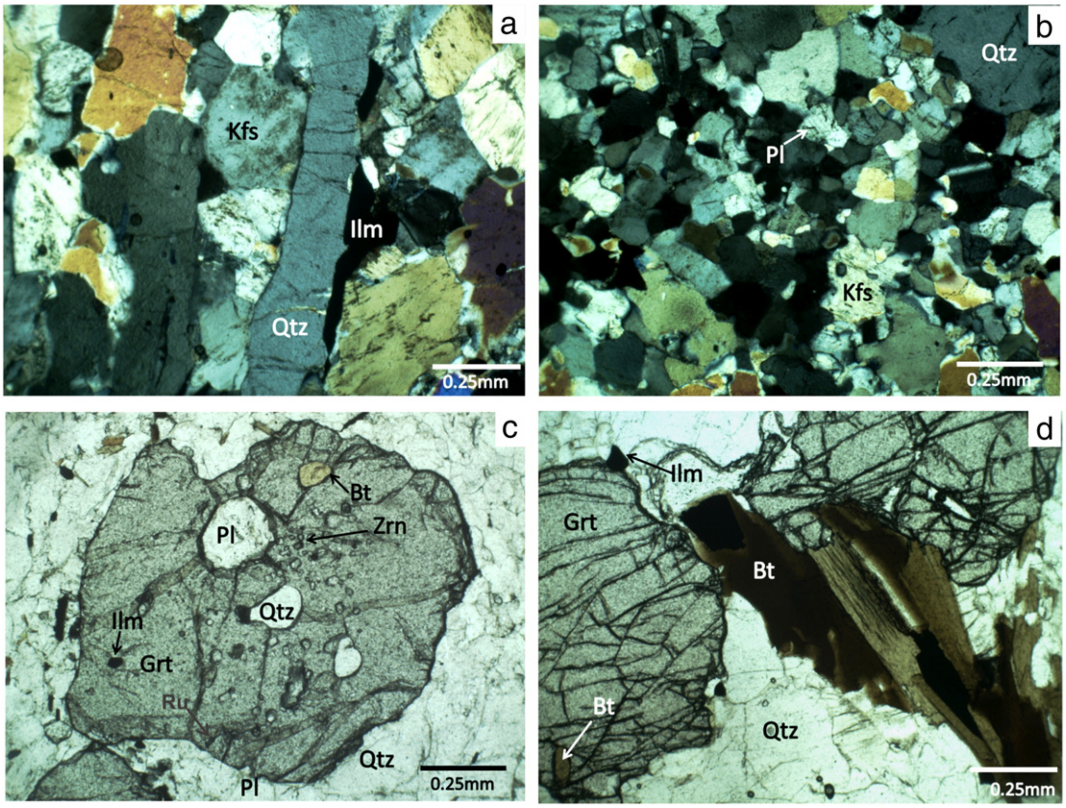

Fig. 6. Photomicrographs showing the main textural features associated with quartz-saturated domains: (a) stretched quartz in the matrix; (b) recrystallized feldspars in the matrix; (c) inclusion phases present in garnet; (d) tiny biotite in the matrix and rimming garnet.

opposite to almandine. The Ca ($CaO = 0.151–0.154$ wt.%) and Ti ($TiO_2 = 0–0.007$ wt.%) contents of Grt_2 are relatively low compared to Grt_1 (Table 1). The average composition of Grt_2 is $Alm_{62.4}Prp_{31.8}Grs_{3.7}Sps_{0.8}Adr_{1.3}$ within the core to $Alm_{59.9}Prp_{34.0}Grs_{2.5}Sps_{0.8}Adr_{2.7}$ at the rim (Table 1).

In the quartz-saturated domains also, garnet is mainly of an almandine–pyrope solid solution, with only small amounts of grossular, spessartine and andradite (Table 2). The average composition of garnet ranges from $Alm_{58.5}Prp_{35.8}Grs_{4.1}Sps_{0.9}Adr_{0.7}$ within the core to $Alm_{62.1}Prp_{32.7}Grs_{3.2}Sps_{0.6}Adr_{1.4}$ at the rim (Table 2). The Ti content of these garnet is $TiO_2 = 0.050–0.070$ wt.% (Table 2).

5.1.2. Feldspars

In the quartz-undersaturated domains, matrix plagioclase is more calcic (An_{51}–$An_{63.5}$) compared to plagioclase inclusions in garnet (An_{34}–An_{44}) and plagioclase inclusions within quartz which are found included in garnet (An_{38}, Table 1). The orthoclase content of the alkali-feldspar included within Grt_1 is slightly higher compared to that of the alkali-feldspar in the matrix (Table 1).

Plagioclase inclusions in garnet and in the matrix of the quartz-saturated domains are albite-rich and show similar compositions (Ab_{66}–Ab_{69}). Orthoclase content of the alkali-feldspar varies from Or_{84}–Or_{92} (Table 2).

5.1.3. Biotite

The X_{Mg} content of biotite varies with textural setting in both quartz-saturated and quartz-undersaturated domains (Tables 1 and 2). In the quartz-undersaturated domains, tiny biotite inclusions (Bt_1) within Grt_1 display the highest X_{Mg} content up to 0.76 and show TiO_2 content of up to 6.99 wt.%. The X_{Mg} content of biotite surrounding garnet porphyroblast (Bt_2) is 0.62–0.59, while the TiO_2 content varies from 6.10 to 5.41 wt.%.

In the quartz-saturated domains, biotite inclusions in garnet contain the highest X_{Mg} content of up to 0.72 and TiO_2 content of up to 6.80 wt.%. The X_{Mg} content of biotite surrounding garnet porphyroblasts is 0.67–0.64, while the TiO_2 content varies from 6.08 to 5.18 wt.%.

5.1.4. Spinel

Spinel is mainly a solid solution of hercynite and Mg-spinel (average $X_{Mg} = 0.37–038$). Spinel inclusions within Grt_2 and in the matrix exhibit similar compositions. The ZnO content of spinel ranges from 2.70 to 2.82 wt.%.

5.1.5. Corundum

Corundum contains minor amounts of FeO (0.32–0.24 wt.%), TiO_2 (0–0.10 wt.%), Cr_2O_3 (0.39–0.70 wt.%) and ZnO (0.03–0.06 wt.%).

5.1.6. Other minerals

Chemical compositions of rutile, ilmenite and sillimanite in the quartz-undersaturated domains are given in Table 1, while rutile and ilmenite compositions in the quartz-saturated domains are given in Table 2.

5.2. Whole rock chemistry

Compositions of the quartz-undersaturated and quartz-saturated domains of pelitic granulites were obtained using a Panalytical Axios wave-length dispersive XRF spectrometer (WDXRF, 2.4 kV) at ETH Zurich, Switzerland. Samples were reduced in grain size with a hydraulic press in a stainless-steel beaker and ground to powder with an agate mill. Standard analyses were performed on fused glass-beads prepared from rock powder mixed with Lithium–Tetraborate (1:5 mixture) using a Claisse M4® fluxer. The calibration is based on ca. 40 certified international standards.

Table 1
Representative electron microprobe analyses of minerals in the quartz-undersaturated domains.

	Garnet$_1$			Garnet$_2$			Spinel		Biotite			Rutile		Ilmenite
	Rim	Mantle	Core	Rim	Mantle	Core	In-Grt$_2$	Next to Crn	In-Grt$_1$	Rim-Grt$_1$		In-Grt$_1$		In-Grt$_1$
										Core	Rim			
SiO_2	39.20	38.70	39.13	38.45	38.56	38.33	0.24	0.07	36.94	36.82	36.96	0.16	0.28	0.09
TiO_2	0.05	0.06	0.10	0.00	0.00	0.01	0.01	0.03	6.99	6.05	5.42	97.82	97.44	52.77
Al_2O_3	22.07	22.11	22.15	22.00	22.26	21.29	59.65	60.41	14.82	14.80	14.86	0.10	0.07	0.00
Cr_2O_3	0.12	0.01	0.05	0.09	0.09	0.05	1.66	0.85	0.41	0.24	0.16	0.07	0.36	0.09
FeO	29.90	28.60	29.04	29.30	29.34	29.06	25.96	25.99	11.11	14.57	16.02	0.52	0.57	44.97
MnO	0.42	0.36	0.33	0.38	0.30	0.35	0.02	0.00	0.012	0.02	0.02	0.00	0.02	0.13
MgO	8.16	8.74	8.88	8.77	8.73	8.18	9.01	8.98	14.91	13.18	12.71	0.04	0.00	2.04
CaO	2.03	2.32	2.14	1.87	1.83	1.80	0.05	0.03	0.05	0.00	0.01	0.05	0.05	0.00
Na_2O	0.00	0.00	0.03	0.00	0.00	0.01	0.04	0.08	0.29	0.02	0.11	0.00	0.03	0.02
K_2O	0.00	0.01	0.00	0.00	0.00	0.00	0.01	0.00	9.46	9.53	9.51	0.03	0.02	0.00
ZnO	0.07	0.00	0.05	0.00	0.00	0.00	2.82	2.70	0.11	0.01	0.03	0.07	0.07	0.00
Total	101.99	100.92	101.89	100.85	101.12	99.07	99.47	99.14	95.11	95.23	95.8	98.86	98.91	100.11
O	12	12	12	12	12	12	4	4	22	22	22	2	2	3
Si	2.989	2.970	2.976	2.961	2.960	3.005	0.007	0.002	5.453	5.505	5.528	0.002	0.004	0.002
Ti	0.003	0.004	0.006	0.000	0.000	0.000	0.000	0.001	0.775	0.680	0.609	0.992	0.988	0.989
Al	1.983	2.000	1.985	1.997	2.014	1.967	1.936	1.961	2.578	2.609	2.62	0.002	0.001	0.000
Cr	0.007	0.001	0.003	0.005	0.005	0.003	0.036	0.018	0.048	0.028	0.019	0.001	0.004	0.002
Fe	1.905	1.836	1.847	1.887	1.883	1.905	0.598	0.599	1.372	1.823	2.003	0.006	0.006	0.937
Mn	0.027	0.023	0.021	0.025	0.020	0.023	0.001	0.000	0.002	0.002	0.003	0.000	0.000	0.003
Mg	0.927	1.000	1.006	1.007	0.998	0.955	0.370	0.369	3.280	2.936	2.833	0.001	0.000	0.076
Ca	0.166	0.190	0.174	0.154	0.151	0.151	0.002	0.001	0.007	0.000	0.001	0.001	0.001	0.000
Na	0.000	0.000	0.004	0.000	0.000	0.001	0.002	0.004	0.083	0.005	0.032	0.000	0.001	0.001
K	0.000	0.001	0.000	0.000	0.000	0.000	0.000	0.000	1.782	1.818	1.815	0.001	0.000	0.000
Zn	0.004	0.000	0.003	0.000	0.000	0.000	0.057	0.055	0.012	0.001	0.003	0.001	0.001	0.000
Tot. cation	8.012	8.026	8.026	8.037	8.031	8.011	3.008	3.010	15.391	15.407	15.466	1.005	1.006	2.009
X_{Mg}	0.327	0.353	0.353	0.348	0.346	0.334	0.382	0.381	0.705	0.617	0.586			
Alm	0.624	0.591	0.595	0.599	0.605	0.624								
Spe	0.009	0.008	0.007	0.008	0.007	0.008								
Prp	0.311	0.337	0.339	0.340	0.337	0.318								
Grs	0.039	0.039	0.033	0.025	0.027	0.037								
Adr	0.017	0.025	0.025	0.027	0.024	0.013								

	Plagioclase					Orthoclase			Corundum		Sillimanite	
	In the matrix			In-Grt$_1$	In-Qtz, Grt$_1$	In-Qtz, Grt$_1$	In-Grt$_1$	Matrix	In-Grt$_2$	Co-Grt$_2$	In-Grt$_2$	In Matrix
	Rim	Mantle	Core									
SiO_2	53.74	54.21	51.06	2.65	58.00	63.89	63.93	63.60	0.13	0.19	36.75	36.68
TiO_2	0.00	0.00	0.02	0.00	0.04	0.05	0.05	0.00	0.10	0.00	0.11	0.07
Al_2O_3	27.72	28.41	29.81	1.33	25.75	18.74	18.69	18.82	97.82	97.89	0.00	0.01
Cr_2O_3	0.08	0.03	0.05	0.00	0.01	0.04	0.05	0.01	0.39	0.70	0.05	0.04
FeO	0.00	0.02	0.05	0.01	0.08	0.06	0.04	0.04	0.32	0.24	0.01	0.00
MnO	0.02	0.02	0.01	0.00	0.03	0.00	0.00	0.03	0.01	0.00	0.00	0.01
MgO	0.02	0.00	0.03	0.00	0.01	0.00	0.00	0.00	0.00	0.01	61.05	60.96
CaO	10.65	10.81	12.96	0.35	7.84	0.04	0.31	0.38	0.00	0.03	0.58	0.70
Na_2O	5.33	5.14	4.02	0.67	6.99	1.49	1.75	1.752	0.00	0.00	0.06	0.07
K_2O	0.23	0.23	0.16	0.01	0.10	14.20	13.72	13.3	0.00	0.00	0.00	0.03
ZnO	0.00	0.00	0.05	0.00	0.00	0.04	0.00	0.03	0.03	0.04	0.01	0.01
Total	97.79	98.87	98.23	98.78	98.84	98.54	98.53	98.04	98.80	99.11	98.62	98.59
O	8	8	8	8	8	8	8	8	3	3	5	5
Si	2.480	2.472	2.362	2.648	2.622	2.978	2.976	2.972	0.002	0.003	1.111	1.110
Ti	0.000	0.000	0.001	0.003	0.001	0.002	0.002	0.000	0.001	0.000	0.002	0.002
Al	1.508	1.527	1.625	1.334	1.372	1.029	1.025	1.037	1.987	1.983	0.000	0.000
Cr	0.003	0.001	0.002	0.000	0.001	0.002	0.002	0.000	0.005	0.010	0.001	0.001
Fe	0.000	0.001	0.002	0.005	0.003	0.002	0.001	0.002	0.005	0.003	0.000	0.000
Mn	0.001	0.001	0.000	0.000	0.001	0.000	0.000	0.001	0.000	0.000	0.000	0.000
Mg	0.001	0.000	0.002	0.000	0.001	0.000	0.000	0.000	0.000	0.000	2.750	2.749
Ca	0.527	0.528	0.643	0.353	0.380	0.002	0.015	0.019	0.000	0.001	0.019	0.023
Na	0.477	0.455	0.360	0.666	0.613	0.134	0.158	0.159	0.000	0.000	0.003	0.004
K	0.013	0.014	0.010	0.014	0.006	0.844	0.815	0.797	0.000	0.000	0.000	0.001
Zn	0.000	0.000	0.002	0.000	0.000	0.001	0.000	0.001	0.000	0.001	0.000	0.000
Tot. cation	5.010	4.998	5.009	5.022	4.999	4.994	4.995	4.988	2.001	2.001	3.888	3.890
An	0.518	0.530	0.635	0.380	0.342	0.002	0.016	0.020				
Ab	0.469	0.456	0.356	0.614	0.645	0.137	0.160	0.163				
Or	0.013	0.014	0.010	0.006	0.014	0.861	0.825	0.818				

In-Grt$_1$ — Inclusions in garnet$_1$, In-Grt$_2$ — Inclusions in garnet$_2$, Rim-Grt$_1$ — rimmed around garnet$_1$, In-Qtz, Grt$_1$ — inclusion in quartz, which occur as inclusion in Grt$_1$, Co-Grt$_2$ — coexisting with garnet$_2$.

Table 2
Representative electron microprobe analyses of minerals in the quartz-saturated domains.

	Garnet			Plagioclase		Orthoclase		Biotite		Rutile	Ilmenite
	Core	Mantle	Rim	Inclusion in garnet	In matrix	Inclusion in garnet	In matrix	Inclusion in garnet	In matrix		
SiO_2	39.25	39.24	39.17	61.83	61.29	66.02	65.91	38.52	37.52	0.11	0.06
TiO_2	0.07	0.05	0.05	0.03	0.01	0.01	0.04	6.80	6.09	98.47	52.62
Al_2O_3	22.51	22.27	22.18	24.82	24.79	18.39	18.57	14.77	14.86	0.00	0.03
Cr_2O_3	0.00	0.00	0.06	0.00	0.00	0.00	0.00	0.09	0.18	0.00	0.04
FeO	27.51	28.33	29.60	0.10	0.07	0.48	0.19	9.40	12.70	0.72	47.16
MnO	0.41	0.36	0.30	0.00	0.00	0.04	0.04	0.00	0.02	0.00	0.04
MgO	9.39	9.39	8.58	0.01	0.00	0.00	0.00	15.95	14.14	0.04	1.16
CaO	1.76	1.58	1.67	6.50	6.45	0.08	0.09	0.01	0.02	0.05	0.07
Na_2O	0.06	0.01	0.03	7.78	8.20	0.79	1.45	0.35	0.15	0.00	0.00
K_2O	0.00	0.00	0.00	0.54	0.19	15.49	14.60	9.37	9.51	0.03	0.03
Total	100.96	101.23	102.64	101.61	101.01	101.31	100.89	95.27	95.19	99.42	101.21
O	12	12	12	8	8	8	8	22	22	2	3
Si	2.986	2.987	2.988	2.710	2.702	3.005	3.000	5.596	5.554	0.001	0.002
Ti	0.004	0.003	0.003	0.001	0.000	0.000	0.002	0.743	0.678	0.994	0.984
Al	2.019	1.999	1.969	1.282	1.288	0.987	0.997	2.529	2.592	0.000	0.001
Cr	0.000	0.000	0.003	0.000	0.000	0.000	0.000	0.010	0.021	0.000	0.001
Fe	1.751	1.804	1.864	0.004	0.003	0.018	0.007	1.142	1.572	0.008	0.981
Mn	0.027	0.023	0.019	0.000	0.000	0.001	0.002	0.000	0.003	0.000	0.001
Mg	1.064	1.065	0.963	0.001	0.000	0.000	0.000	3.454	3.119	0.001	0.043
Ca	0.143	0.129	0.135	0.305	0.305	0.004	0.004	0.002	0.003	0.001	0.002
Na	0.009	0.002	0.004	0.661	0.701	0.070	0.128	0.099	0.043	0.000	0.000
K	0.000	0.000	0.000	0.030	0.011	0.900	0.848	1.762	1.796	0.000	0.001
Total cation	8.004	8.012	8.012	4.994	5.010	4.986	4.988	15.358	15.381	0.000	2.014
X_{Mg}	0.378	0.371	0.341					0.752	0.665	1.005	
Alm	0.585	0.592	0.621								
Spe	0.009	0.008	0.006								
Prp	0.358	0.357	0.327								
Grs	0.041	0.030	0.032								
Adr	0.007	0.013	0.014								
An				0.306	0.300	0.004	0.004				
Ab				0.663	0.690	0.072	0.131				
Or				0.030	0.010	0.924	0.865				

Bulk rock compositions are given in Table 3 and discussed in terms of X_{Mg}, A/AFM and S/SFM following the approach of Harley (2008).

Quartz-undersaturated domains of pelitic granulites display a SiO_2 content of ca. 45 wt.% (S/SFM = 44), are rich in Al_2O_3 (ca. 25 wt.%, A/AFM = 26), FeO (ca. 17 wt.%) and TiO_2 (ca. 1.5 wt.%). The CaO, Na_2O and K_2O contents are 4 wt.%, 2.3 wt.% and 1.2 wt.%, respectively. Compared to the quartz-undersaturated domains, the quartz-saturated domains are rich in SiO_2 (ca. 60 wt.%, S/SFM = 61) but poor in Al_2O_3 (ca. 17 wt.%, A/AFM = 20), FeO (ca. 10 wt.%), TiO_2 (ca. 1 wt.%) and CaO (ca. 3 wt.%). The Na_2O and K_2O contents are 2.8 wt.% and 1.2 wt.%, respectively. Both quartz-undersaturated and saturated domains show similar X_{Mg} values of 0.29 and 0.31, respectively. Considering trace element composition, the quartz-undersaturated domains are richer in Ba, Sr, Zr, Cr and V than the quartz-saturated domains.

6. Textural evolution

6.1. Quartz-undersaturated domains

Part of the early metamorphic history of the studied pelitic granulites is disclosed by inclusions in Grt_1-porphyroblasts. In the quartz-undersaturated domains, Bt_1 inclusions within Grt_1 are considerably rich in Ti (up to 7 wt.%), suggesting that the consumption of Ti-rich biotite during prograde metamorphism may have led to the formation of Ti-rich Grt_1, similar to those described by O'Brien et al. (1997) for granulites from the Sudetes. Further, the occurrence of quartz, Ti-rich Bt_1, An-poor plagioclase and rare sillimanite as inclusions in Grt_1, suggests the occurrence of the prograde melting reaction.

$$Bt_1 + Sil + Qtz + An\,poor\text{-}Pl = Grt_1 + Kfs + An\,rich\text{-}Pl + Melt. \qquad (1)$$

Table 3
Representative bulk chemical compositions of quartz-undersaturated and quartz-saturated domains in the pelitic granulite.

Samples	Quartz-undersaturated domains	Quartz-saturated domains
wt.%		
SiO_2	44.93	59.95
TiO_2	1.47	1.06
Al_2O_3	24.68	17.48
FeO	16.86	10.92
MnO	0.14	0.12
MgO	3.88	2.76
CaO	4.07	3.06
Na_2O	2.28	2.82
K_2O	1.21	1.22
P_2O_5	0.09	0.12
Cr_2O_3	0.04	0.02
LOI	0.32	0.51
Total	99.97	100.20
X_{Mg}	0.29	0.31
ppm		
Rb	35.0	47.5
Ba	600.4	337.4
Sr	301.9	223.4
Nb	40.1	22.5
Zr	471.2	192.8
Y	56.7	33.5
Zn	93.2	67.5
Cu	75.4	51.2
Ni	73.2	47.2
Cr	283	107.3
V	267.7	212.2
Sc	38.2	25.7
Th	33.9	25.8
U	1.6	1.2

The presence of both spinel and Bt_1 inclusions in Grt_1 can be explained by the melting reaction:

$$Bt_1 + Sil = Grt_1 + Spl + Kfs + Melt. \quad (2)$$

The melting reaction (1) completely consumed quartz from the rock matrix, while both biotite-consuming reactions (1) and (2) may have concurred to consume all of biotite during prograde fluid-absent melting. The peak-mineral assemblage of the quartz-undersaturated parts of pelitic granulites was Ti-rich-garnet–plagioclase–alkali-feldspar–spinel–sillimanite.

The occurrence of both spinel and sillimanite inclusions in Grt_2 (Fig. 5g), coexisting with corundum (Fig. 5a to g) and the association of garnet, corundum, spinel and sillimanite in the matrix (Fig. 5f) may be explained via the post-peak reaction:

$$Spl + Sil = Grt_2 + Crn. \quad (3)$$

Corundum coexisting with Grt_2 (Fig. 5a to g), partially embedded corundum grains within the rim area of Grt_2 (Fig. 5a to c), corundum inclusions in Grt_2 (Fig. 5a and b) and the presence of rare spinel inclusions within corundum (Fig. 5h) confirm the occurrence of reaction (3). The low Ti- and Ca-contents displayed by Grt_2 compared to those of Grt_1 (Table 1) and the lack of rutile needles in Grt_2 suggest that Grt_1 and Grt_2 have formed at different *P*–*T* conditions.

Late Bt_2 surrounding garnet-porphyroblasts (Figs. 3d and 4e) are relatively Fe-rich and poorer in Mg and Ti than Bt_1 inclusions in Grt_1 (Table 1). Bt_2 probably formed during retrogression in the presence of fluid/melt by the reaction:

$$Grt_1 + fluid/melt = Bt_2. \quad (4)$$

6.2. Quartz-saturated domains

The presence of Bt_1 and quartz inclusions within garnet suggests that fluid-absent biotite melting reaction:

$$Bt_1 + Qtz \pm Pl = Grt + Kfs + Melt \quad (5)$$

which took place during prograde rock evolution. Due to quartz-rich bulk composition, reaction (5) may have occurred only as far as all the biotites (but not all the quartz) were completely consumed from the rock. The peak assemblage of the domains is composed of quartz–plagioclase–alkali-feldspar–garnet. Late Bt_2 surrounding garnet-porphyroblasts (Fig. 6d) could probably have formed during retrogression in the presence of fluid/melt by reaction (4), similar to those of the quartz-undersaturated domains.

7. *P–T* estimates

7.1. Prograde metamorphic conditions

The reconstruction of the *PT* path during the prograde evolution is particularly challenging in granulite-facies rocks because of overprinting of early assemblages by peak/post-peak minerals and resetting of phase compositions and/or changes in the bulk composition through addition or loss of melts. Nevertheless, mineral assemblages preserved as inclusions in large porphyroblasts, usually garnet, may provide information on at least a portion of the rock's prograde history. Here, we quantify part of the prograde path of pelitic granulites using the pressure independent Ti-in-Biotite thermometer of Henry et al. (2005), the Hoisch (1990) calibrations of the GBPQ geobarometer and the Koziol and Newton (1988) calibration of the GASP geobarometer.

Bt_1 grains included in Grt_1 in the quartz-undersaturated domains display a TiO_2 content of about 7 wt.% and a X_{Mg} of ca. 0.7 corresponding to an estimated *T* of 835 °C using the Henry et al. (2005) calibration of the Ti-in-Biotite thermometer and assuming no ferric iron in the biotite structure (Table 4). The estimated temperatures would increase up to 842 °C and 848 °C given incorporation of 10% and 20% ferric iron in biotite, respectively. Bt_1 inclusions in garnet of the quartz-saturated domains display a TiO_2 content up to 6.80 wt.% and a X_{Mg} of ca. 0.75, corresponding to an estimate *T* of 845 °C (Table 4).

In the quartz-undersaturated domains, the Hoisch (1990) calibrations of the GBPQ-(Mg) and GBPQ-(Fe) barometers calculated using Grt_1 core composition and Bt_1 inclusions are estimated to be $P = 10$, 10.4 and 10.7 and 10.6, 11 and 11.4 at nominal $T = 825$, 850 and 875 °C, respectively (Table. 4). In the quartz-saturated domains, garnet core composition and Bt_1 inclusions yielded $P = 10.6$, 10.9 and 11.3 and 11.3, 11.7 and 12.2 for nominal $T = 825$, 850 and 875 °C, respectively (Table 4).

The Koziol and Newton (1988) calibration of the GASP (garnet–sillimanite–plagioclase–quartz) geobarometer calculated using Grt_1 core composition and the composition of plagioclase grains included adjacent to quartz in the core area of Grt_1 in the quartz-undersaturated domains yielded $P = 9.9$, 10.3, 10.8 and 11.2 kbar at nominal $T = 825$, 850 and 875 °C, respectively (Table 4).

7.2. Peak metamorphic conditions

Peak-metamorphic conditions were calculated using two complementary approaches: pseudosection and conventional geothermobarometry. Pseudosections were calculated for both quartz-undersaturated and quartz-saturated domains of pelitic granulites in the chemical system NCKFMASHTMnO, with the software of Perplex_X_07 (Connolly, 2005), using the 2004 update of the Holland and Powell (1998) internally-consistent thermodynamic database and mineral solution models as listed in the Fig. 7 and 8 captions. The modeled bulk rock compositions are taken from XRF analysis (Table 3). As P_2O_5 is not taken into account in the calculations, the CaO content equivalent to apatite has been subtracted from the measured bulk rock composition. H_2O content was taken as correspondent to the loss on ignition (LOI). To have an estimate of the Fe_2O_3 bulk content, we calculated T–$X(Fe_2O_3)$ pseudosections at a pressure of 10 kbar (Figs. 7a and 8a).

In the T–$X(Fe_2O_3)$ section constructed for the quartz-undersaturated domain (Fig. 7a), the observed peak assemblage of garnet–plagioclase–alkali-feldspar–spinel–sillimanite–ilmenite is predicted to be stable for $X(Fe_2O_3)$ comprised between 0.08 and 0.30 and temperatures varying between 950 and 1050 °C (see bold field in Fig. 7a). Higher $X(Fe_2O_3)$ values would progressively stabilize magnetite instead of spinel, while at lower $X(Fe_2O_3)$ and *T* corundum would appear. At higher *T*, sillimanite or alkali-feldspar would not be stable for $X(Fe_2O_3) < 0.11$ or >0.11, respectively.

The *P*–*T* pseudosection of Fig. 7b displays phase relations for the quartz-undersaturated composition calculated at $X(Fe_2O_3) = 0.15$. The observed peak assemblage is stable for a wide *PT* window, ranging between 875–1070 °C and 6–11 kbar (see bold field in Fig. 7b). At $P < 6$ kbar, cordierite is predicted to be stable. At *P* between 6 and 8.5–9 kbar, decreasing *T* would stabilize biotite, while increasing *T* would consume sillimanite. At $P > 8.5$–9 kbar, a decrease of *T* would produce corundum and an increase of *T* would destabilize alkali-feldspar. On the basis of textural evidences indicating that after the peak of the metamorphism corundum and Grt_2 formed at the expense of spinel and sillimanite (reaction 3), we suggest that peak conditions in the quartz-undersaturated domains occurred at $T > 950$ °C and $P \gtrsim 9$ kbar.

In the quartz-saturated domain, the observed peak assemblage is constituted by quartz–plagioclase–alkali-feldspar–garnet–ilmenite–melt. The T–$X(Fe_2O_3)$ section calculated at $P = 10$ kbar (Fig. 8a) suggests that $X(Fe_2O_3)$ was <0.15–0.25 (depending on *T*) and peak *T* was between about 860 and 1010 °C (see bold field in Fig. 8a). At higher

Table 4
Conventional thermobarometric data calculated for the quartz-saturated and quartz-undersaturated domains.

Mineral compositions	Si	Ti	Mg	Fe^{2+}	Mn	Ca	Na	K	Nominal T (°C)	Calculated P (kbar)	Calculated T (°C)	Reference*
Prograde												
Quartz-undersaturated domains												
Biotite inclusion		0.775	3.280	1.372							835	{1}
Garnet$_1$ core			0.927	1.864	0.027	0.166			825	9.4$^{(Sil)}$		{2}
Plagioclase**						0.380	0.620	0.010	850	9.8$^{(Sil)}$		{2}
Biotite inclusion$^{(O = 12)}$***	2.974	0.423	1.789	0.748	0.001	0.004	0.045	0.972	875	10.2$^{(Sil)}$		{2}
									825	10$^{(Mg)}$/10.6$^{(Fe)}$		{3}
									850	10.4$^{(Mg)}$/11$^{(Fe)}$		{3}
									875	10.7$^{(Mg)}$/11.4$^{(Fe)}$		{3}
Quartz-saturated domains												
Biotite inclusion												{1}
Garnet$_1$ core												
Plagioclase**									825	10.6$^{(Mg)}$/11.3$^{(Fe)}$		
Biotite inclusion$^{(O = 12)}$*		0.380	1.955	0.575	0.000		0.052	0.961	850	10.9$^{(Mg)}$/11.7$^{(Fe)}$		{3}
									875	11.3$^{(Mg)}$/12.2$^{(Fe)}$		{3}
Near peak conditions												
Quartz-undersaturated domains												
Garnet$_1$	2.979$^{(Av)+}$	0.0040$^{(Av)+}$									948$^{(Av)+}$	{4}
									900	8.1		{5}
									950	9.2		{5}
									1000	10.4		{5}
Quartz-saturated domains												
Garnet	2.992$^{(Av)+}$	0.0037$^{(Av)+}$									941$^{(Av)+}$	{4}
									900	8.0		{5}
									950	9.1		{5}
									1000	10.3		{5}
Isobaric cooling												
Quartz-undersaturated domains												
Garnet$_2$			0.995	1.889	0.022	0.153			800	6.1		{6}
Spinel			0.370	0.598					900	8.2		{6}
									1000	10.3		{6}
Matrix biotite		0.680	2.936								800	{1}
Quartz-saturated domains												
Matrix biotite		0.674	3.114								812	{1}

$^{(Av)+}$: Average.

* {1} Ti in Biotite geothermometer (Henry et al., 2005); {2} $^{(Sil)}$Grt–Sil–Pl–Qtz geobarometer (Koziol and Newton, 1988); {3} $^{(Mg)}$Grt–Bt–Pl–Qtz: (Mg) geobarometer (Hoisch, 1990), $^{(Fe)}$Grt–Bt–Pl–Qtz: (Fe) geobarometer (Hoisch, 1990);{4}Ti in Grt geothermometer (Kawasaki and Motoyoshi, 2007); {5}Ti in Grt geobarometer (Kawasaki and Motoyoshi, 2007); {6} Grt–Crn–Spl–Sil geobarometer (Shultere and Bohlen, 1988).

** Plagioclase: plagioclase inclusions in the core of Garnet.

*** Biotite inclusion$^{(O = 12)}$: for oxygen number 11.

$X(Fe_2O_3)$ values, sillimanite and then magnetite would be stable, while at higher and lower temperatures alkali-feldspar would disappear and biotite would appear, respectively.

In the P–T diagram of Fig. 8b calculated at $X(Fe_2O_3) = 0.10$, the observed peak assemblage is stable at $T = 870$–1040 °C and $P > 8$ kbar (see bold field in Fig. 8b). At $P < 8$ kbar, orthopyroxene would appear and be part of the peak assemblage. At $T < 860$–870 °C, our model predicts biotite as a stable mineral phase, while at >960–1040 °C (depending on P) alkali-feldspar would disappear. Thus, estimated peaks of P–T inferred from the quartz-saturated rock domains, although covering a wide area in the P–T space, are consistent with those derived from the quartz-undersaturated domains.

Combining the P–T estimates inferred from pseudosections calculated for both quartz-undersaturated and quartz-saturated parts, we suggest that metamorphic peak temperature occurred around at least 950–975 °C and at pressures around 9–9.5 kbar.

Peak P–T conditions were also calculated using the empirically calibrated Ti-in-Garnet geothermometer (pressure independent) and geobarometer of Kawasaki and Motoyoshi (2007). P–T estimates using average Grt$_1$ core composition of the quartz-undersaturated domains yielded a temperature of 948 °C and a pressure of 9.2 kbar at nominal $T = 950$ °C. The same thermometer applied for average garnet core composition of the quartz-saturated domains yielded a similar temperature of 941 °C and pressure of 9.1 kbar at $T = 950$ °C. These P–T conditions are in good agreement with estimates from pseudosections.

7.3. Post-peak conditions

Textural evidences suggest that after metamorphic peak in the quartz-undersaturated portions of the pelitic granulites a second generation of garnet (Grt$_2$) has formed together with corundum at the expense of sillimanite and spinel (Fig. 5). This observation indicates that the investigated granulite experienced a phase of nearly isobaric cooling after the peak of temperature. In fact, as shown by the pseudosection of Fig. 7b, corundum is stable exclusively at $P > 8.5$ kbar and $T \gtrsim 900$ °C. If after peak-T the rock evolved along a decompressional path, corundum would not form and, at about 6 kbar, cordierite would be produced instead. Similarly, the pseudosection calculated for the quartz-saturated composition predicts the appearance of orthopyroxene already at $P < 8$ kbar and cordierite at $P < 5$ kbar in a temperature range of 860–970 °C, again excluding considerable decompression after peak-T.

We explored more in detail the formation of corundum and Grt$_2$ calculating the modal amounts of spinel, sillimanite, corundum and garnet expressed in vol.%. Fig. 9 shows that along an isobaric cooling path (outlined by black arrows in the diagrams) at about 920–930 °C and 9–9.5 kbar corundum appears and spinel disappears contemporaneously. At the same P–T conditions, our model predicts a decrease of sillimanite and an increase of garnet content. This indicates that reaction (3) inferred from textural observations is effectively reproduced by thermodynamic modelling. The experimental calibration

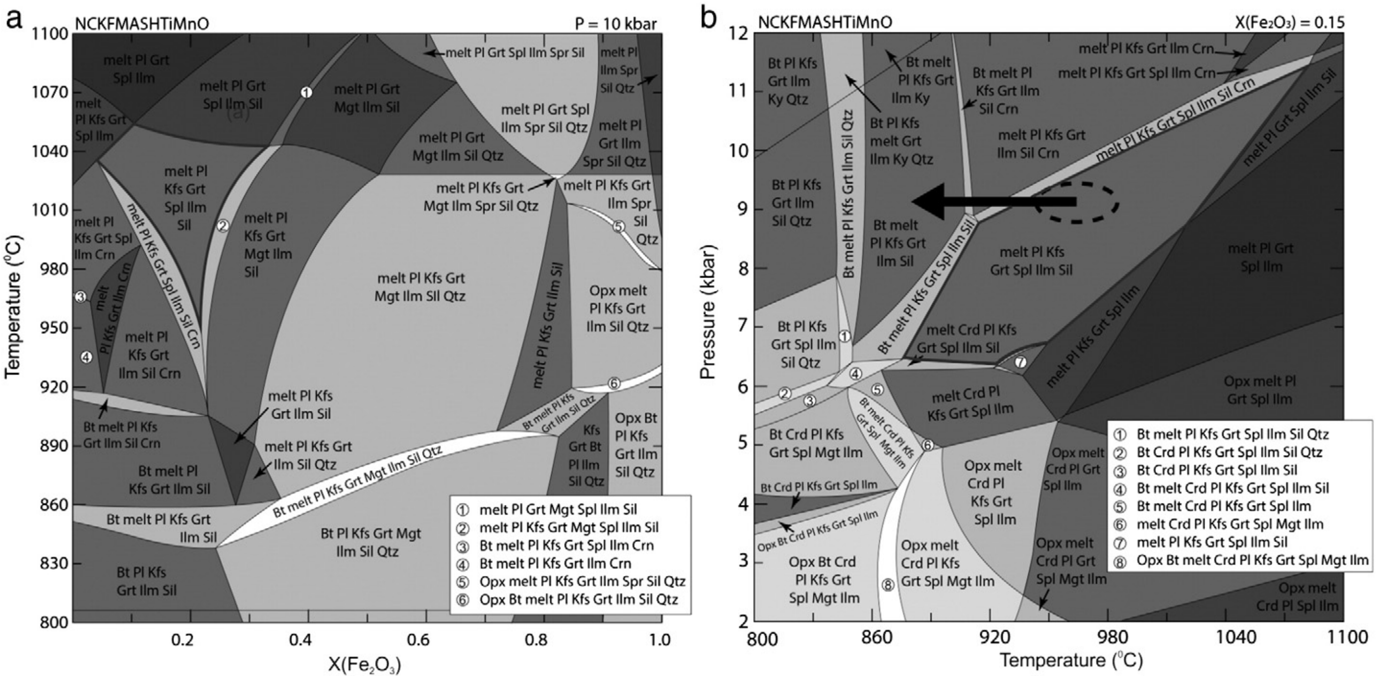

Fig. 7. (a) *T*–*X*(Fe_2O_3) pseudosection calculated in the NCKFMASHTMnO system at $P = 10.0$ kbar for the quartz-undersaturated composition of pelitic granulites; (b) *P*–*T* pseudosection calculated at $X(Fe_2O_3) = 0.15$ for the quartz-undersaturated composition; solution-phase models used in the calculations are: garnet — Gt(WPH): White et al. (2007); biotite — Bio(TCC): Tajčmanová et al. (2009); sapphirine — Sapp(Tp): Taylor-Jones and Powel (2010); ilmenite — Ilm(WHP): White et al. (2000); alkali-feldspar — San: Waldbaum and Thompson (1969); plagioclase — Pl(h): Newton et al. (1980); orthopyroxene — Opx(HP): Powell and Holland (1999); spinel — Sp(WPC): White et al. (2002); cordierite — hCrd: Holland and Powell (1998); melt — melt (HP): White et al. (2007).

of reaction (3) of Shultere and Bohlen (1988) calculated using Grt_2 core and spinel compositions (Table 4), yielded $P = 6.1$, 8.2, 10.3 kbar at nominal $T = 800$, 900 and 1000 °C, respectively (see Fig. 10). This estimate is in good agreement with the results of our thermodynamic modelling.

The Ti-in-Biotite thermometer of Henry et al. (2005) applied using the compositions of retrograde biotite (Bt_2) which is present in the matrix and surrounding garnet assuming that there is no ferric iron in the biotite structure (Table 4), yielded *T* up to 800 °C and 815 °C in the quartz-undersaturated and saturated domains, respectively.

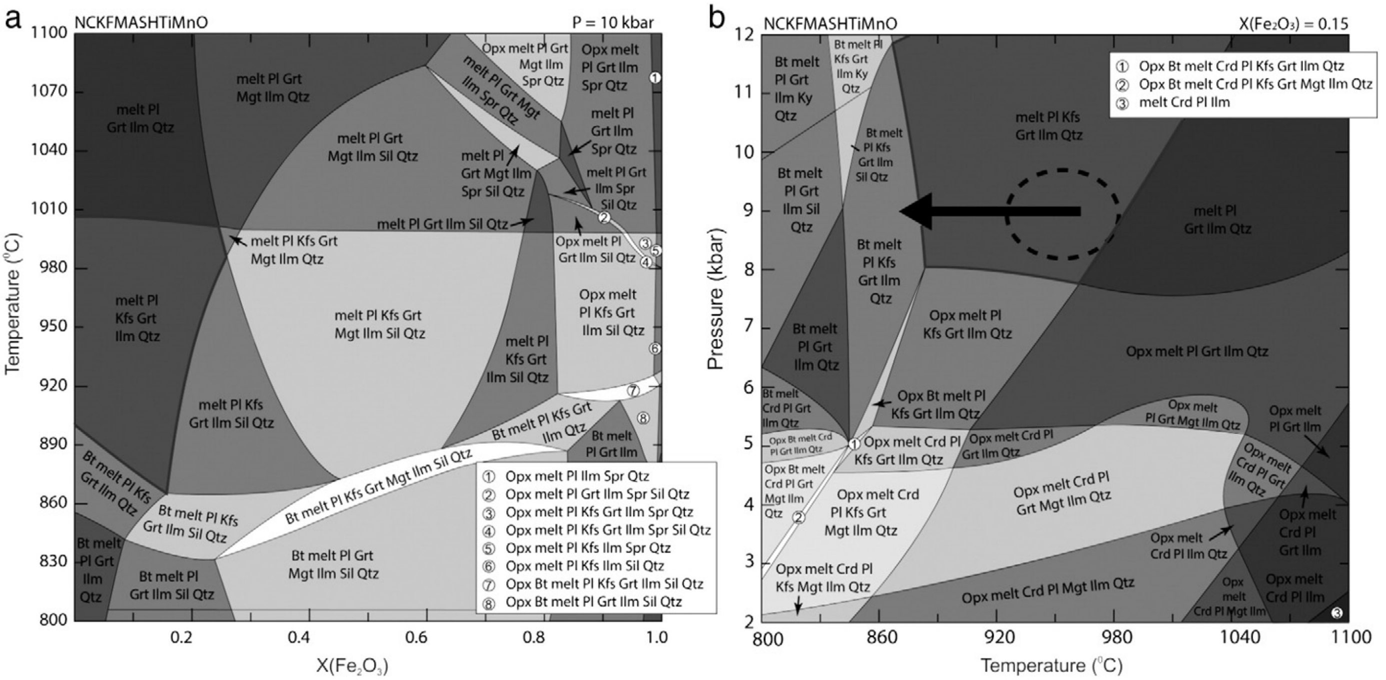

Fig. 8. (a) *T*–*X*(Fe_2O_3) pseudosection at $P = 10.0$ kbar for the quartz-saturated composition of pelitic granulites; (b) *P*–*T* pseudosection calculated at $X(Fe_2O_3) = 0.10$ for quartz-saturated composition. Solution-phase models used in the calculations are: garnet — Gt(WPH): White et al. (2007); biotite — Bio(TCC): Tajčmanová et al. (2009); sapphirine — Sapp(Tp): Taylor-Jones and Powel (2010) ilmenite — Ilm(WHP); White et al. (2000); alkali-feldspar — San: Waldbaum and Thompson (1969); plagioclase — Pl(h): Newton et al. (1980); orthopyroxene — Opx(HP): Powell and Holland (1999) and White et al. (2002); cordierite — hCrd: Holland and Powell (1998); melt — melt (HP): White et al. (2007).

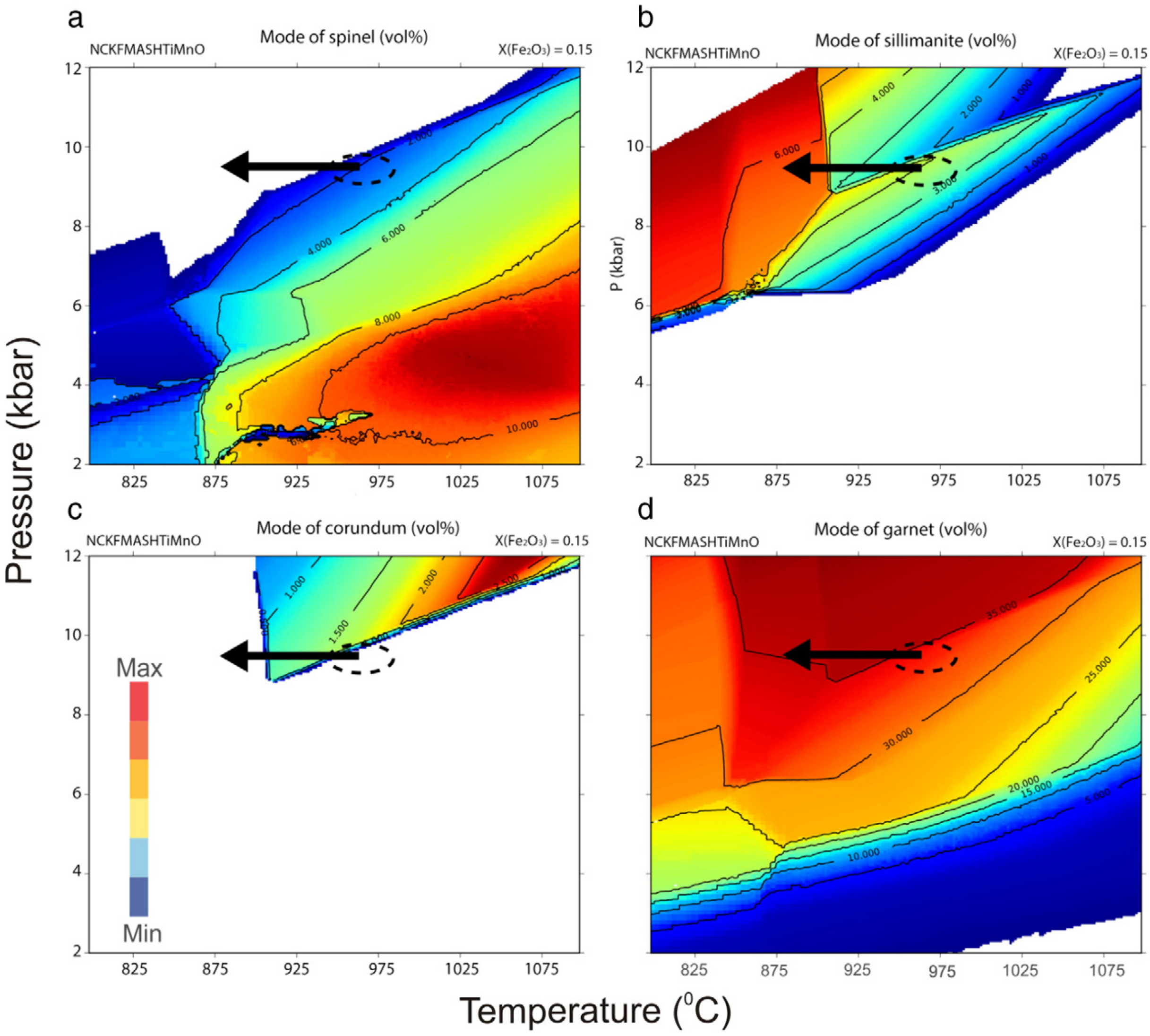

Fig. 9. PT-diagrams showing the modal proportion of spinel (a), sillimanite (b), corundum (c) and garnet (d) expressed in vol.% calculated in the NCKFMASHTMnO system for the quartz-undersaturated pelitic granulite composition. Dashed ellipses correspond to the estimated *P*–*T* peak conditions calculated from *P*–*T* pseudosections and Ti-in-Grt geothermobarometry; black arrows display the inferred post-peak *P*–*T* path.

8. Discussion

The two rock domains display a clear contrast in terms of bulk chemistry: quartz-saturated domain richer in SiO_2 and poorer in Al_2O_3 compared to those of the quartz undersaturated domain. Trace element compositions also show appreciable difference in bulk chemistry (see Table 3). Interbedding of metasediments of pelitic and more psammitic or intermediate composition is a common feature in the basement rocks and has also been reported extensively from the Highland Complex of Sri Lanka (e.g., Dharmapriya et al., 2014). Therefore, compositional differences between the quartz-saturated and quartz-undersaturated rock domains may reflect a primary heterogeneity in the sedimentation during deposition.

8.1. P–T evolution of the UHT pelitic granulite of the HC

The chemistry of minerals preserved as inclusions in Grt_1 suggests that the studied pelitic granulite attained a maximum *P* of 10.5–11 kbar probably at *T* around 850 °C during its prograde history. In the quartz-undersaturated rock domains, during further heating probably Qtz was completely consumed by reaction (1) from the rock-matrix leading to the formation of large Grt_1 porphyroblasts as a peritectic phase. The occurrence of rear spinel inclusion in the mantle to rim within Grt_1 suggests that the melting reaction (2) was initiated after the consumption of Qtz from the rock. Thus, a series of heat-induced fluid-absent biotite–melting reactions may have progressively consumed both biotite and quartz from the rock matrix and produced large Grt_1-porphyroblasts and spinel.

Hiroi et al. (1994) argued that the prograde path experienced by many pelitic granulites of the Highland Complex of Sri Lanka passed from the kyanite to the sillimanite stability field. Evidence for that are rare kyanite–hercynite inclusions in garnet from metapelitic granulites sampled close to the Nawalapitiya area. However, we did not observe kyanite in our samples.

Both pseudosections and conventional geothermobarometry suggest that peak metamorphic temperature reached UHT conditions of 950–975 °C and pressures of 9–9.5 kbar (Fig. 7 and Table 4). Metamorphic peak was followed by a period of isobaric cooling responsible for the formation of corundum and a second generation of garnet (Grt_2) at about 930 °C, as well as exsolution of rutile needles and apatite rods from Grt_1 (Fig. 4a, b, c, d, e, f and h). Further, nearly isobaric cooling formed late biotite (Bt_2) mainly at the rim of large Grt_1-porphyroblasts

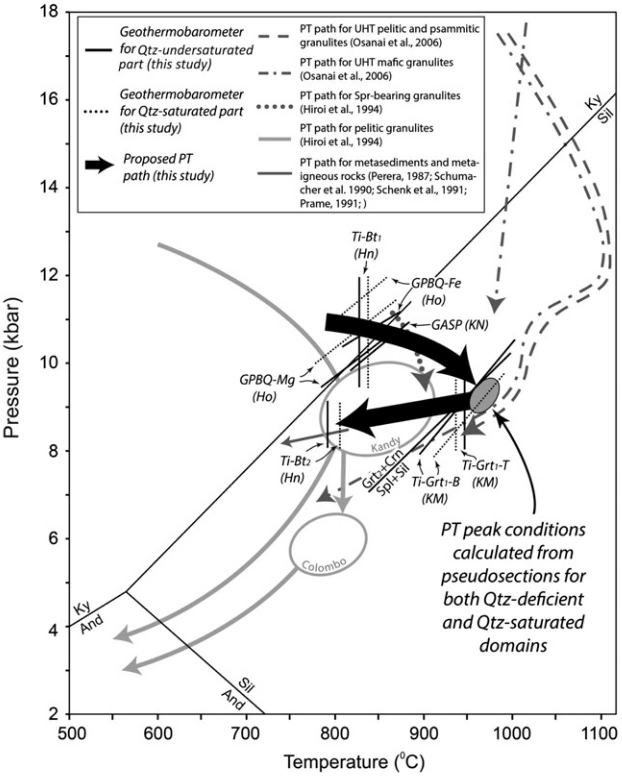

Fig. 10. Combined *P–T* path obtained from this study with proposed *P–T* trajectory for high grade granulites from previous studies.

at $T = {\sim}800$ °C by reaction (4). Bt_2 developed only locally, probably due to the limited availability of metamorphic fluids/melts during retrogression.

Regardless of several occurrences of UHT rocks in restricted localities, the tectonic mechanism for UHT metamorphism in the HC is still unclear. Osanail et al. (1997) suggested that the UHT granulites in the HC may represent residual compositions after partial melting of metapelite under low fO_2 condition. Gondwana terrains located close to Sri Lanka, namely Lützow Holm Complex, east Antarctica (e.g., Motoyoshi and Ishikawa, 1997; Satish-Kumar et al., 2007), southern India (e.g., Collins et al., 2014; Santosh et al., 2003, 2006a) and southern Madagascar (e.g., Janardhan, 1999; Jöns and Schenk, 2011) also display evidence for local occurrences of Neoproterozoic–Cambrian UHT metamorphic rocks. However, further detailed petrological, geochemical and geochronological studies require correlating the relation among these UHT metamorphic rocks.

Fig. 9 displays a possible *P–T*-path for the investigated pelitic granulites and it is compared with those proposed for high-grade granulites including UHT rocks by previous studies in the HC, Sri Lanka. The proposed trajectory coincides with the *P–T* paths commonly suggested by previous works on the HC granulites (e.g., Hiroi et al., 1994; Ogo et al., 1992; Perera, 1987; Schumacher et al., 1990). Early high pressure conditions result mostly from crustal over-thickening during a continent–continent collision (e.g. Sandiford et al., 1988). Relict kyanite associated with sapphirine, spinel, corundum, staurolite and quartz occurring as inclusions in garnet in many pelitic granulites also reveals earlier high-pressure conditions before metamorphic peak temperature is attained in the HC (Hiroi et al., 2014). Subsequently, lower crustal extension could have taken place in consequence of non-coaxial flow, resulting in a decompressional event accompanied by increasing temperature up to the peak of the metamorphism. The major lineation is defined by pervasive stretching in the HC granulites formed during non-coaxial strain of D_2 deformation event which has taken place simultaneously with the peak metamorphism (e.g., Kehelpannala, 1997; Kriegsman, 1994). This observation provides evidence for the existence of strong lower crustal shear stresses near the peak of metamorphism.

Many studies have documented the occurrence of a late stage isothermal decompression after a period of isobaric cooling following peak-*T*, mostly expressed by symplectitic textures involving the formation of cordierite at the expense of garnet and sillimanite (e.g., Ogo et al., 1992; Perera, 1984). Nevertheless, the samples investigated in this study show no evidences for a late stage of isothermal decompression. White et al. (2007) suggested that mineral assemblages in dry rocks would hardly react in response to *P–T* changes and hence, post-peak textures would not form in the absence of fluids/melts infiltrating though the rock after the metamorphic peak.

8.2. Significance of the garnet + corundum assemblage

In general, the assemblage garnet + corundum in pelitic rocks of high X_{Mg} bulk composition is interpreted as indicative of high pressure and temperature conditions (e.g., Kelsey et al., 2006; Osanai et al., 1998; Shimpo et al., 2006; Tsunogae and Santosh, 2007). Coexisting garnet and corundum have been reported from UHP rocks, aluminous eclogites, kimberlites, as well as numerous granulite terrains worldwide which experienced UHT conditions of 900–1050 °C at relatively high but not eclogitic pressures of 10–12 kbar (Horrocks, 1983; Moraes et al., 2002; Osanai et al., 1998; Ouzegane et al., 2003; Sengupta et al., 1999; Shimpo et al., 2006). However, Kelsey et al. (2006) demonstrated that garnet + corundum bearing assemblages may occur at a *P* of around 8 kbar and a *T* of 850–900 °C in relatively iron- and alumina-rich bulk compositions.

In the central HC, Ogo et al. (1992) reported corundum inclusions associated with relict kyanite and staurolite in garnet-porphyroblasts from khondalites. Large patches of garnet, sapphirine and corundum in the matrix of a sapphirine-bearing pelitic granulite boulder and spinel + corundum inclusions in garnet are reported from the same rock type (Kriegsman and Schumacher, 1999). However, garnet and corundum in these samples occur rarely in mutual contact. Osanai et al. (2006) found coexisting garnet + corundum in the matrix of quartzofeldspathic granulites and reported corundum + quartz and relict kyanite inclusions in garnet, suggesting that the rock reached a *P* of around 12 kbar and $T > 1100$ °C.

In the present study, a lack of corundum in the matrix or as inclusions in Grt_1-porphyroblasts, which is the main peritectic phase produced during prograde melting, suggests that corundum was not present during the prograde evolution. In contrast, textural observations coupled with thermodynamic modeling shows that garnet + corundum formed during an isobaric cooling stage rather than at peak *P* or during decompression along a clockwise *P–T*-path.

Therefore, the investigated pelitic granulites provide a rare evidence for formation of garnet + corundum after peak *T* along a retrograde metamorphic trajectory under UHT conditions. This is further supported by the lack of pyroxene and also aluminous phases such as cordierite, sapphirine and/or staurolite minerals which are commonly observed in garnet + corundum bearing pelitic granulites elsewhere in the world. The absence of the above minerals could probably be due to the Al and Fe rich but Mg poor (Table 3) bulk chemical composition.

8.3. Significance of rutile needles with ilmenite and apatite rods in Ti rich Grt_1

The clusters and oriented rutile and apatite needles together with ilmenite in Grt_1 (Fig. 5a–i) give indirect clues for the rock's evolution under (relatively HP and UHT) metamorphic conditions. Similar textures have been reported from Ultrahigh Pressure (UHP) metamorphic rocks (e.g., Griffin, 2008; Zhang et al., 2003), high to UHT granulites (e.g., Kawasaki and Motoyoshi, 2000; Kawasaki et al., 2011; Marschall et al., 2003; O'Brien and Rötzler, 2003; Osanai et al., 2001) and mantle derived rocks such as peridotites (e.g., Obata, 1994; Song et al., 2004). Exsolution of apatite rods is also reported from HP–UHP metamorphic rocks elsewhere (Ague et al., 2012; Zhang et al., 2003).

Proyer et al. (2013) argued that rutile formation from garnet cannot occur in a closed system and require substantial chemical exchange by solid-state diffusion between the garnet and the rock matrix. Nevertheless, experimental studies have shown that TiO_2 could dissolve into silicates like garnet and orthopyroxene at high temperatures (e.g., Kawasaki and Motoyoshi, 2007) and Ti solubility in garnet increases with increasing *P* and *T* (e.g., Zhang et al., 2003). Subsequently, during retrograde cooling and/or decompression, TiO_2 may precipitate as needle- or rod-like rutile crystals within the host mineral (Ague et al., 2012; Kawasaki and Motoyoshi, 2007; Song et al., 2004; Wark and Watson, 2006).

Occurrence of Ti-rich biotite (TiO_2 up to 7 wt.%) exclusively as inclusions in Ti-rich Grt_1-porphyroblasts suggests that Ti-rich Grt_1 formed via reaction (1), which completely consumed Ti-rich biotite from the matrix. Thus, the enrichment of Ti in Grt_1 could result from the consumption of Ti-rich biotite during the prograde evolution of the rock. Hence, we infer that precipitation of rod-like rutile and ilmenite observed in the pelitic granulites may have occurred during isobaric cooling, probably simultaneously with the formation of corundum + Grt_2 at UHT conditions.

9. Conclusions

The chemistry of minerals preserved as inclusions in the core of Grt_1 indicates that during the prograde history of pelitic granulite peak a *P* of 10.5–11 kbar at *T* around 850 °C was attained. Further heating during extension may have induced a series of fluid-absent biotite–melting reactions which have progressively consumed biotite and quartz from the matrix and produced porphyroblastic garnet and spinel. Textural observations coupled with both pseudosections calculated in the NCKFMASHTMnO system and Ti-in-Garnet geothermobarometry suggest that the rock has reached peak metamorphic temperatures of 950–975 °C and pressures of 9–9.5 kbar.

Peak *T* was followed by a period of isobaric cooling forming corundum and Grt_2 via the reaction Spl + Sil = Grt_2 + Crn at around 930 °C. Thermodynamic modelling confirms that corundum appears and spinel contemporaneously disappears at about 920–930 °C and 9–9.5 kbar along an isobaric cooling path. At the same *P*–*T* conditions, our model predicts a decrease of sillimanite and an increase of garnet content. The exsolution of rutile needles and apatite rods in Grt_1 also could have taken place simultaneously with the formation of Grt_2 + Crn. Further isobaric cooling produced a second generation of biotite at the rim of large Grt_1-porphyroblasts at ca. 800 °C.

Hence, the investigated pelitic granulites provide a rare example for coexistence of garnet + corundum along a retrograde metamorphic trajectory under UHT conditions. This suggests that isobaric cooling at the base of the crust is an alternative process to explain the formation of coexisting garnet + corundum, especially in the absence of cordierite and/or orthopyroxene.

Acknowledgments

We are grateful to the National Research Council (NRC) of Sri Lanka (Grant No. NRC-11-180) for the funding. Field travel was extensively supported by the Ministry of Technology and Research, Sri Lanka (Grant No. MTR/TRD/AGR/3/1/04 of the Indo-Lanka Joint Research on High Temperature Lower Crust of East Central Gondwana). Partial support for the sample analysis by the National Natural Science Foundation of China (Grant No. 41173011) and ETH Zurich, Switzerland is gratefully acknowledged. Dr. K. Sajeev and Dr. Jan Kihle are highly thanked for the detailed and constructive comments and suggestions to improve this manuscript. Prof. Marco Scambelluri is thanked for the editorial work and valuable comments and suggestions to improve this manuscript. We thank Mr. S. Opatha and Miss Thilini Harischandra at the Institute of Fundamental Studies (IFS) for the technical help and support in preparing the petrographic thin sections, respectively. We also appreciate Mr. Qian Mao and Yuguang Ma at the Institute of Geology and Geophysics, Chinese Academy of Sciences for the EPMA analysis.

References

Ague, J.J., Eckert, James O., Jr, J.O., 2012. Precipitation of rutile and ilmenite needles in garnet: implications for extreme metamorphic conditions in the Acadian Orogen, U.S.A. American Mineralogist 97, 840–855.

Ater, P.C., Eggler, D.H., Callum, M.E., 1984. Petrology and geochemistry of mantle eclogite xenoliths from Colorado–Wyoming kimberlites: recycled ocean crust? Kimberlite: II. The Mantle and Crust–Mantle Relationships. Elsevier, Amsterdam, pp. 309–318

Baba, S., 2003. Two stages of sapphirine formation during prograde and retrograde metamorphism in the Paleoproterozoic Lewisian complex in south Harris, NW Scotland. Journal of Petrology 44, 329–354.

Caporuscio, F.A., Morse, S.A., 1978. Occurrence of sapphirine plus quartz at Peekskill, New York. American Journal of Science 278, 1334–1342.

Chinner, G.A., Dixon, R.D., 1973. Irish osumilite. Mineralogical Magazine 39, 189–192.

Collins, A.S., Clark, C., Plavsa, D., 2014. Peninsular India in Gondwana: the tectonothermal evolution of the Southern Granulite Terrain and its Gondwanan counterparts. Gondwana Research 25, 190–203.

Connolly, J.A.D., 2005. Computation of phase equilibria by linear programming: a tool for geodynamic modelling and its application to subduction zone decarbonation. Earth and Planetary Science Letters 236, 524–541.

Cooray, P.G., 1994. The Precambrian of Sri Lanka: a historic review. Precambrian Research 66, 3–18.

Dasgupta, D., Sengupta, P., Ehl, J., Raith, M., Bardhan, S., 1995. Reaction textures in a suite of spinel granulites from the eastern Ghats Belt, India: evidence for polymetamorphism, a partial petrogenetic grid in the system KFMASH and the roles of ZnO and Fe_2O_3. Journal of Petrology 36, 345–461.

Dharmapriya, P.L., Malaviarachchi, S.P.K., Galli, A., Su, B., Subasinghe, N.D., Dissanayake, C.B., Nimalsiri, T.B., Zhu, B., 2014. P–T evolution of a spinel + quartz bearing khondalite from the Highland Complex, Sri Lanka: implications for non-UHT metamorphism. Journal of Asian Earth Sciences 95, 99–113.

Ellis, D.J., 1980. Osumilite–sapphirine–quartz granulites from Enderby Land, Antarctica — P–T conditions of metamorphism, implications for garnet–cordierite equilibria and the evolution of the deep crust. Contributions to Mineralogy and Petrology 74, 201–210.

Faulhaber, S., Raith, M., 1991. Geothermometry and geobarometry of high-grade rocks: a case study on garnet–pyroxene granulites in southern Sri Lanka. Mineralogical Magazine 55, 17–40.

Fernando, W.I.S., Iizumi, S., 2001. Rb–Sr whole rock-mineral isochron ages of plutonic rocks from the Wanni Complex, Sri Lanka. Gondwana Research 4, 113–120.

Galli, A., Le Bayon, B., Schmidt, M.W., Burg, J.P., Caddick, M.J., Reusser, E., 2010. Granulites and charnockites of the Gruf Complex: evidence for Permian ultra-high temperature metamorphism in the Central Alps. Lithos 124, 17–45.

Geological Survey Department of Sri Lanka, 1996. Geological Map of Sri Lanka Colombo: Geological Survey Department of Sri Lanka Scale 1:100000, sheets No14.

Griffin, W.L., 2008. Major transformations reveal Earth's deep secrets. Geology 36, 95–96.

Griffin, W.L., Jensen, B.B., Misra, S.N., 1971. Anomalously elongated rutile in eclogite-facies pyroxene and garnet. Norsk Geologisk Tidsskrift 51, 177–185.
Hacker, B.R., Sharp, T., Zhang, R.Y., Liou, J.G., Hervig, R.L., 1997. Determining the origin of ultrahigh-pressure lherzolites. Science 278, 702–704.

Harley, S.L., 1998. On the occurrence and characterization of ultrahigh temperature crustal metamorphism. In: Treloar, P.J., O'Brien, P.J. (Eds.), What Drives Metamorphism and Metamorphic Relations?. Special Publications. Geological Society, London, pp. 81–107.

Harley, S.L., 2008. Refining the P–T records of UHT crustal metamorphism. Journal of Metamorphic Geology 26, 125–154.

Harley, S.L., Motoyoshi, Y., 2000. Al zoning in orthopyroxene in a sapphirine quartzite: evidence for N1120 degrees C UHT metamorphism in the Napier Complex, Antarctica, and implications for the entropy of sapphirine. Contributions to Mineralogy and Petrology 138, 293–307.

Henry, D.J., Guidotti, C.V., Thomson, J.A., 2005. The Ti-saturation surface for low-to medium pressure metapelitic biotites: implications for geothermometry and Ti substitution mechanism. American Mineralogist 90, 316–328.

Hiroi, Y., Ogo, Y., Namba, K., 1994. Evidence for prograde metamorphic evolution of Sri Lankan pelitic granulites, and implications for the development of continental crust. Precambrian Research 66, 245–263.

Hiroi, Y., Yanagi, A., Kato, M., Kobayashi, T., Prame, B., Hokada, T., Satish-Kumar, M., Ishikawa, M., Adachi, T., Osanai, Y., Motoyoshi, Y., Shiraishi, K., 2014. Supercooled melt inclusions in lower-crustal granulites as a consequence of rapid exhumation by channel flow. Gondwana Research 25, 226–234.

Hö1zl, S., Köhler, H., Kröner, A., Jaeckel, P., Liew, T.C., 1991. Geochronology of the Sri Lankan basement. In: KrOner, A. (Ed.), The Crystalline Crust of Sri Lanka, Part I. Summary of Research of the German-Sri Lankan Consortium. Geological Survey. Department Sri Lanka, Professional. Paper 5, pp. 6–257.

Hö1zl, S., Hofmann, A.W., Todt, W., Krönler, H., 1994. U–Pb geochronology of the Sri Lanka basement. In: Raith, M., Hoernes, S. (Eds.), Tectonic, Metamorphic and Isotopic Evolution of Deep Crustal Rocks, With Special Emphasis on Sri Lanka. Precambrian Research 66, pp. 123–149.

Hoisch, T.D., 1990. Empirical calibration of six geobarometers for the mineral assemblage quartz + muscovite + biotite + plagioclase + garnet. Contributions to Mineralogy and Petrology 104, 225–234.

Holland, T.J.B., Powell, R., 1998. An internally consistent thermodynamic dataset for phases of petrological interest. Journal of Metamorphic Geology 16, 309–343.

Horrocks, P., 1983. A corundum and sapphirine paragenesis from the Limpopo Mobile Belt, southern Africa. Journal of Metamorphic Geology 1, 13–23.

Janardhan, A.S., 1999. Southern granulite terrain, south of the Palghat–Cauvery shear zone: implications for India–Madagascar connection. Gondwana Research 2, 463–469.

Jöns, N., Schenk, Y., 2011. The ultrahigh temperature granulites of southern Madagascar in a polymetamorphic context: implications for the amalgamation of the Gondwana supercontinent. European Journal of Mineralogy 23, 127–156.

Kawasaki, T., Motoyoshi, Y., 2000. High-pressure and high-temperature phase relations of an orthopyroxene granulite from McIntyre Island, Enderby Land, East Antarctica. Polar Geoscience 13, 114–133.

Kawasaki, T., Motoyoshi, Y., 2007. Solubility of TiO_2 in garnet and orthopyroxene: Ti thermometer for ultrahigh-temperature granulites. In: Cooper, A.K., et al. (Eds.), Antarctica: A Keystone in a Changing World, USGS Open-file Report 2007-1047, Short Research Paper 038.

Kawasaki, T., Nakano, N., Osanai, Y., 2011. Osumilite and a spinel + quartz association in garnet–sillimanite gneiss from Rundvågshetta, Lützow-Holm Complex, East Antarctica. Gondwana Research 19, 430–445.

Kehelpannala, K.V.W., 1997. Deformation of a high-grade Gondwana fragment, Sri Lanka. Gondwana Research 1, 47–68.

Kelly, N.M., Harley, S.L., 2004. Orthopyroxene–corundum in Mg–Al-rich granulites from the Oygarden Islands, East Antarctica. Journal of Petrology 45, 1481–1512.

Kelsey, D.E., 2008. On ultrahigh-temperature crustal metamorphism. Gondwana Research 13, 1–29.

Kelsey, D.E., Clark, C., Hand, M., Collins, A.S., 2006. Comment on "First report of garnet–corundum rocks from southern India: implications for prograde high pressure (eclogite–facies?) metamorphism". Earth and Planetary Science Letters 249, 529–534.

Koziol, A.M., Newton, R.C., 1988. Redetermination of the anorthite breakdown reaction and improvement of the plagioclase–garnet–Al_2SiO_5, geobarometer. American Mineralogist 73, 216–223.

Kretz, R., 1983. Symbols for rock-forming minerals. American Mineralogist 68, 277–279.

Kriegsman, L.M., 1994. Evidence for a fold nappe in the high-grade basement of central Sri Lanka: terrane assembly in the Pan-African lower crust. In: Raith, M., Hoernes, S. (Eds.), Tectonic, Metamorphic and Isotopic Evolution of Deep Crustal Rocks, With Special Emphasis on Sri Lanka. Precambrian Research 66, pp. 59–76.

Kriegsman, L.M., Schumacher, J.C., 1999. Petrology of sapphirine bearing and associated granulites from central Sri Lanka. Journal of Petrology 40, 1211–1239.

Kröner, A., Cooray, P.G., Vitanage, P.W., 1991. Lithotectonic subdivision of the Precambrian basement in Sri Lanka. In: Körner, A. (Ed.), The Crystalline Crust of Sri Lanka, Part-1. Summary of Research of the German–Sri Lankan Consortium. Geological Survey Department, Sri Lanka, Professional Papers 5, pp. 5–21.

Kröner, A., Jaeckel, P., Williams, I.S., 1994. Pb-loss patterns in zircons from a high-grade metamorphic terrain as revealed by different dating methods: U–Pb and Pb–Pb ages for igneous and metamorphic zircons from northern Sri Lanka. Precambrian Research 66, 151–181.

Kröner, A., Kehelpannala, K.V.W., Hegner, E., 2003. Ca. 700–1000 Ma magmatic events and grenvillian-age deformation in Sri Lanka: relevance for rodinia supercontinent formation and dispersal, and Gondwana amalgamation. Journal of Asian Earth Sciences 22, 279–300.

Kröner, A., Santosh, M., Wong, J., 2012. Zircon ages and Hf isotopic systematics reveal vestiges of Mesoproterozoic to Archaean crust within the late Neoproterozoic–Cambrian high-grade terrain of southernmost India. Gondwana Research 21, 876–886.

Kröner, A., Rojas-Agramonte, Y., Kehelpannala, K.V.W., Zack, T., Hegner, E., Geng, H.Y., Wong, J., Barth, M., 2013. Age, Nd–Hf isotopes, and geochemistry of the Vijayan Complex of eastern and southern Sri Lanka: A Grenville-age magmatic arc of unknown derivation. Precambrian Research 234, 288–321.

Malaviarachchi, S.P.K., Takasu, A., 2011a. Electron microprobe dating of Monazites from Sri Lanka. Journal of the Geological Society of Sri Lanka 14, 81–90.

Malaviarachchi, S.P.K., Takasu, A., 2011b. Petrology of metamorphic rocks from the Highland and Kadugannawa Complexes, Sri Lanka. Journal of the Geological Society of Sri Lanka 14, 103–122.

Marschall, H.R., Kalt, A., Hanel, M., 2003. P–T evolution of a Variscan lower-crustal segment: a study of granulites from the Schwarzwald, Germany. Journal of Petrology 44, 227–253.

Martignole, J., Martelat, J.E., 2003. Regional-scale Grenvillian-age UHT metamorphism in the Mollendo-Camana Block (basement of the Peruvian Andes). Journal of Metamorphic Geology 21, 99–120.

Mathavan, V., Fernando, G.W.A.R., 2001. Reactions and textures in grossular–wollastonite–scapolite calc-silicate granulites from Maligawila, Sri Lanka. Lithos 59, 217–232.

Milisenda, C.C., Liew, T.C., Hoffman, A.W., Kröner, A., 1988. Isotopic mapping of age provinces in Precambrian high-grade terrains: Sri Lanka. Journal of Geology 96, 608–615.

Milisenda, C.C., Liew, T.C., Hofmann, A.W., Köler, H., 1994. Nd isotopic mapping of the Sri Lankan basement: update, and additional constraints from Sr isotopes. Precambrian Research 66, 95–110.

Moraes, R., Brown, M., Fuck, R.A., Camargo, M.A., Lima, T.M., 2002. Characterization and P–T evolution of melt-bearing ultrahigh-temperature granulites: an example from the Anapolis–Itaucu Complex of the Brasilia Fold Belt, Brazil. Journal of Petrology 43, 1673–1705.

Morishita, T., Arai, S., Gervilla, F., 2001. High-pressure aluminous mafic rocks from the Ronda peridotite massif, southern Spain: significance of sapphirine- and corundum-bearing mineral assemblages. Lithos 57, 143–161.

Morse, S.A., Talley, J.H., 1971. Sapphirine reactions in deep-seated granulites near Wilson Lake, Central Labrador, Canada. Earth and Planetary Science Letters 10, 325–328.

Motoyoshi, Y., Ishikawa, M., 1997. Metamorphic and structural evolution of granulites from Rundvågshetta, Lützow-Holm Bay, east Antarctica. In: Ricci, C.A. (Ed.), The Antarctic Region: Geological Evolution and Processes: Proceedings of the VII International Symposium on the Antarctic Earth Sciences. Terra Antarctica, Siena, pp. 65–72.

Newton, R.C., Charlu, T.V., Kleppa, O.J., 1980. Thermochemistry of the high structural state plagioclases. Geochemica et Cosmochimica Acta 44, 933–941.

O'Brien, P.J., Rötzler, J., 2003. High-pressure granulites: formation, recovery of peak conditions and implications for tectonics. Journal of Metamorphic Geology 21, 3–20.

O'Brien, P.J., Kröner, A., Jaeckel, P., Hegner, E., Zelazniewicz, A., Kryza, R., 1997. Petrological and isotopic studies on Palaeozoic high-pressure granulites, Go'ry Sowie Mts, Polish Sudetes. Journal of Petrology 38, 433–456.

Obata, M., 1994. Material transfer and local equilibria in a zoned kelyphite from a garnet pyroxenite, Ronda, Spain. Journal of Petrology 35, 271–287.

Ogo, Y., Hiroi, Y., Prame, K.B.N., Motoyoshi, Y., 1992. A new insight of possible correlation between the Lutzow-Holm bay granulites (East Antarctica) and the Sri Lankan granulites. In: Yoshida, et al. (Eds.), Recent Progress in Antarctic Earth Science, pp. 75–86.

Osanai, Y., 1989. A preliminary report on sapphirine/kornerupine granulite from Highland series, Sri Lanka (extended abstract). Seminar on recent advantages in Precambrian Geology of Sri Lanka. IFS Kandy, Sri Lanka.

Osanai, Y., Hamamoto, T., Maishima, O., Kagami, H., 1998. Sapphirine-bearing granulites and related high-temperature metamorphic rocks from the Higo metamorphic terrain, west-central Kyushu, Japan. Journal of metamorphic geology 16, 53–66.

Osanai, Y., Ando, K.T., Miyashita, Y., Kusachi, I., Yamasaki, T., Doyama, D., Prame, W.K.B.N., Jayatilake, S., Mathavan, V., 2000. Geological field work in the southwestern and central parts of the Highland complex, Sri Lanka during 1998–1999, special reference to the highest grade metamorphic rocks. Journal of Geoscience, Osaka City University 43, 227–247.

Osanai, Y., Toyoshima, T., Owada, M., Tsunogae, T., Hokada, T., Crowe, A., Kusachi, I., 2001. Ultrahigh temperature sapphirine–osumilite and sapphirine–quartz granulites from Bunt Island in the Napier Complex, East Antarctica — reconnaissance estimation of P–T evolution. Polar Geosciences 14, 1–24.

Osanai, Y., Sajeev, K., Owada, M., Kehelpannala, K.V.W., Prame, W.K.B., Nakano, N., Jayatileke, S., 2006. Metamorphic evolution of ultrahigh-temperature and high-pressure granulites from Highland Complex, Sri Lanka. Journal of Asian Earth sciences 28, 20–37.

Osanail, Y., Miyashita, Y., Hamamoto, T., 1997. Detailed analyses of partial melting process in pelitic granulites from the southwestern part of Highland Complex, Sri Lanka. Gondwana Research (Gondwana Newsletter Section) l, 157–158.

Ouzegane, K., Boumaza, S., 1996. An example of ultrahigh temperature metamorphism: orthopyroxene–sillimanite–garnet, sapphirine–quartz and spinel–quartz paragenesis in Al–Mg granulites from In Hihaou, In Ouzzal, Hoggar. Journal of Metamorphic Geology 14, 693–708.

Ouzegane, K., Guiraud, M., Kienast, J.R., 2003. Prograde and retrograde evolution in high-temperature corundum granulites (FMAS and KFMASH systems) from In Ouzzal terrane (NW Hoggar, Algeria). Journal of Petrology 44, 517–545.

Perera, L.R.K., 1984. Coexisting cordierite–almandine: a key to the metamorphic history of Sri Lanka. Precambrian Research 25, 349–364.

Perera, L.R.K., 1987, Petrogenesis of granulite-facies metamorphic rocks in Sri Lanka, Unpublished Mphil. Thesis, University of Peradeniya.

Powell, R., Holland, T.J.B., 1999. Relating formulations of the thermodynamics of mineral solid solutions: activity modelling of pyroxenes, amphiboles and micas. American Mineralogist 84, 1–14.

Prame, W.K.B.N., 1991. Metamorphism and nature of the granulite-facies crust in southwestern Sri Lanka: characterization by pelitic/psammopelitic rocks and associated granulites. In: Kraner (Ed.), The Crystalline Crust of Sri Lanka, Part I, Summary of Research of the German–Sri Lankan Consortium. Geological survey Department. Sri Lanka, Prof. Paper 5, pp. 188–199.

Proyer, A., Habler, G., Abart, R., Wirth, R., Krenn, K., Hoinkes, G., 2013. TiO_2 exsolution from garnet by open-system precipitation: evidence from crystallographic and shape preferred orientation of rutile inclusions. Contributions to Mineralogy and Petrology 166, 211–234.

Raase, R., Schenk, V., 1994. Petrology of granulite facies metapelites o f the Highland Complex, Sri Lanka: implications for metamorphic zonation and P–T path. Precambrian research 66, 265–294.

Sajeev, K., Osanai, Y., 2004a. Osumilite and spinel + quartz from Sri Lanka: implications for UHT conditions and retrograde P–T path. Journal of Mineralogical and Petrological Sciences 99, 320–327.

Sajeev, K., Osanai, Y., 2004b. Ultrahigh-temperature metamorphism (1150 °C, 12 kbar) and multi-stage evolution of Mg, Al rich granulites from the central Highland Complex, Sri Lanka. Journal of Petrology 45, 1821–1844.

Sajeev, K., Osanai, Y., Connolly, J.A.D., Suzuki, S., Ishioka, J., Kagami, H., Rino, S., 2007. Extreme crustal metamorphism during a Neoproterozoic event in Sri Lanka, a study of dry mafic granulites. Journal of Geology 115, 563–582.

Sajeev, K., Osanai, Y., Kon, Y., Itaya, T., 2009. Stability of pargasite during ultrahigh-temperature metamorphism: a consequence of titanium and REE partitioning? American Mineralogist 94, 535–545.

Sajeev, K., Williams, I.S., Osanai, Y., 2010. Sensitive high-resolution ion microprobe U–Pb dating of prograde and retrograde ultrahigh-temperature metamorphism as exemplified by Sri Lankan granulites. Geological Society Of America 38, 971–974.

Sandiford, M., Powell, R., 1986. Pyroxene exsolution in granulites from Fyfe Hills, Enderby Land, Antarctica: evidence for 1000 °C metamorphic temperatures in Archean continental crust. American Mineralogist 71, 946–954.

Sandiford, M., Powell, R., Martin, S.F., Perera, L.R.K., 1988. Thermal and baric evolution of garnet granulites from Sri Lanka. Journal of Metamorphic Geology 6, 351–364.

Santosh, M., Yokoyama, K., Biju-Sekhar, S., Rogers, J.J.W., 2003. Multiple tectonothermal events in the granulite blocks of southern India revealed from EPMA dating: implications on the history of supercontinents. Gondwana Research 6, 27–61.

Santosh, M., Morimoto, T., Tsutsumi, Y., 2006a. Geochronology of the khondalite belt of Trivandrum Block, southern India: electron probe ages and implications for Gondwana tectonics. Gondwana Research 9, 261–278.

Santosh, M., Sajeev, K., Li, J.H., 2006b. Extreme crustal metamorphism during Columbia supercontinent assembly: evidence from North China Craton. Gondwana Research 10, 256–266.

Santosh, M., Tsunogae, T., Li, J.H., Liu, S.J., 2007. Discovery of sapphirine-bearing Mg–Al granulites in the North China Craton: implications for Paleoproterozoic ultrahigh temperature metamorphism. Gondwana Research 11, 263–285.

Santosh, M., Tsunogae, T., Malaviarachchi, Sanjeewa P.K., Zhang, Zeming, Ding, Huixia, Tang, Li, Dharmapriya, P.L., 2014. Neoproterozoic crustal evolution in Sri Lanka: insights from petrologic, geochemical and zircon U–Pb and Lu–Hf isotopic data and implications for Gondwana assembly. Precambrian Research 255, 1–29.

Satish-Kumar, M., Motoyoshi, Y., Dunkley, D.J., 2007. Metamorphic evolution of UHT calc-silicate rocks from Rundvågshetta, Lützow-Holm Complex (LHC), East Antarctica. In: Cooper, A.K., Raymond, C.R., et al. (Eds.), Antarctica: A Keystone in a Changing World — Online Proceedings of the 10th ISAES X (USGS Open-File Report 2007-1047, Extended Abstract 082).

Schenk, V., Raase, P., Schumacher, R., 1991. Metamorphic zonation and P–T history of the Highland Complex in Sri Lanka. In: Krbner (Ed.), The Crystalline Crust of Sri Lanka, Part I, Summary of Research of the German–Sri Lankan Consortium. Geological survey Department. Sri Lanka, Prof. Paper 5, pp. 150–163.

Schumacher, R., Faulhaber, S., 1994. Summary and discussion of P–T estimates from garnet–pyroxene–plagioclase–quartz-bearing granulite-facies rocks from Sri Lanka. Precambrian Research 66 (295–30).

Schumacher, R., Schenk, V., Raase, P., Vitanage, P.W., 1990. Granulite-facies metamorphism of metabasic and intermediate rocks in the Highland Series of Sri Lanka. In: Ashworth, J.R., Brown, M. (Eds.), Crustal Anatexis. Unwin Hyman, London, pp. 235–271.

Sengupta, P., Sen, J., Dasgupta, S., Raith, M., Bhui, U.K., Ehl, J., 1999. Ultra-high temperature metamorphism of metapelitic granulites from Kondapalle, Eastern Ghats Belt: implications for the Indo-Antarctic correlation. Journal of Petrology 40, 1065–1087.

Shaw, R.K., Arima, M., 1996. High temperature metamorphic imprint on calc silicate granulites of Rayagada, Eastern Ghats, India: implication for the isobaric cooling path. Contributions to Mineralogy and Petrology 126, 169–180.

Shimpo, M., Tsunogae, T., Santosh, M., 2006. First report of garnet–corundum rocks from southern India: implications for prograde high-pressure (eclogite facies?) metamorphism. Earth and Planetary Science Letters 242, 111–129.

Shultere, J., Bohlen, S., 1988. The stability of hercynite and hercynite–gahnite spinels in corundum- or quartz-bearing assemblage. Journal of Petrology 30, 1017–1031.

Song, S., Zhang, L., Niu, Y., 2004. Ultra-deep origin of garnet peridotite from the North Qaidam ultrahigh-pressure belt, northern Tibetan Plateau, NW China. American Mineralogist 89, 1330–1336.

Su, B.X., Zhang, H.F., Deloule, E., Sakyi, P.A., Xiao, Y., Tang, Y.J., Hu, Y., Ying, J.F., Liu, P.P., 2012. Extremely high Li and low δ^7Li signatures in the lithospheric mantle. Chemical Geology 292–293, 149–157.

Tajčmanová, L., Connolly, J.A.D., Cesare, B., 2009. A thermodynamic model for titanium and ferric iron solution in biotite. Journal of Metamorphic Geology 27, 153–165.

Taylor-Jones, K., Powel, R., 2010. The stability of sapphirine + quartz: calculated phase equilibria in FEO–MgO–Al_2O_3–SiO_2–TiO_2–O. Journal of Metamorphic Geology 28, 615–633.

Tsunogae, T., Santosh, M., 2007. Ultrahigh-temperature metamorphism in southern Indian granulite terrane. International Association of Gondwana Research Memoir 10, 1–21.

Tsunogae, T., Santosh, M., Osanai, Y., Owada, M., Toyoshima, T., Hokada, T., 2002. Very high density carbonic fluid inclusions in sapphirine bearing granulites from Tonagh Island in the Archean Napier Complex, East Antarctica: implications for CO_2 infiltration during ultrahigh-temperature ($T > 1100$ °C) metamorphism. Contributions to Mineralogy and Petrology 143, 279–299.

Tsunogae, T., Osanai, Y., Owada, M., Toyoshima, T., Hokada, T., Crowe, W.A., 2003. High fluorine pargasites in ultrahigh temperature granulites from Tonagh Island in the Archean Napier Complex, East Antarctica. Lithos 70, 21–38.

Waldbaum, D.R., Thompson, J.B.J., 1969. Mixing properties of sanidine crystalline solutions: IV. Phase diagrams from equation of state. American Mineralogist 54, 1274–1298.

Wark, D.A., Watson, E.B., 2006. TitaniQ: a titanium-in-quartz geothermometer. Contributions to Mineralogy and Petrology 152, 743–754.

White, R.W., Powell, R., Holland, T.J.B., Worley, B.A., 2000. The effect of TiO_2 and Fe_2O_3 on metapelitic assemblages at greenschist and amphibolite facies conditions: mineral equilibria calculations in the system K_2O–FeO–MgO–Al_2O_3–SiO_2–H_2O–TiO_2–Fe_2O_3. Journal of Metamorphic Geology 18, 497–511.

White, R.W., Powell, R., Clarke, G.L., 2002. The interpretation of reaction textures in Fe-rich metapelitic granulites of the Musgrave Block, central Australia: constraints from mineral equilibria calculations in the system K_2O–FeO–MgO–Al_2O_3–SiO_2–H_2O–TiO_2–Fe_2O_3. Journal of Metamorphic Geology 20, 41–55.

White, R.W., Powell, R., Holland, T.J.B., 2007. Progress relating to calculation of partial melting equilibria for metapelites. Journal of Metamorphic Geology 25, 511–527.

Willbold, M., Hegner, E., Kleinschrodt, R., Stosch, H.-G., Kehelpannala, K.V.W., Dulski, P., 2004. Geochemical evidence for a Neoproterozoic magmatic continental mar-gin in Sri Lanka-relevence for the Rodinia-Gondwana supercontinental cycle. Precambrian Research 130, 185–198.

Zhang, R.Y., Zhai, S.M., Fei, Y.W., Liou, J.G., 2003. Titanium solubility in coexisting garnet and clinopyroxene at very high pressure: the significance of exsolved rutile in garnet. Earth and Planetary Science Letters 216, 591–601.

Zhang, R.Y., Liou, J.G., Zheng, J.P., 2004. Ultrahigh-pressure corundum rich garnetite in garnet peridotite, Sulu terrane, China. Contributions to Mineralogy and Petrology 147, 21–31.